ON SECOND ORDER WAVE LOADING AND RESPONSE IN IRREGULAR SEAS

R. EATOCK TAYLOR and M. P. KERNOT*

Department of Engineering Science, University of Oxford, Parks Road, Oxford OX1 3PJ, U. K.

Wave drift responses at low frequencies and springing at high frequencies can both be modelled as second order processes, involving terms proportional to the square of the wave elevation in irregular seas. Although the models of both these phenomena share many common features, springing introduces several additional complexities. These concern both the second order hydrodynamic analysis, and the probabilistic modelling of the resulting first plus second order responses. This article highlights these in the context of springing, which is particularly relevant to the design of Tension Leg Platforms and offshore structures susceptible to lightly damped resonant responses, at periods in the range from around 2 to 5 seconds. The three closely linked aspects of hydrodynamics, spectral analysis and probabilistic modelling are considered, and sample numerical results discussed.

1 Introduction

Despite the undoubted successes achieved in the design of offshore structures on the basis of linear hydrodynamics, it is now generally understood that the model offered by linear theory is often inadequate. There are important physical phenomena, having impact on the design of fixed and floating structures, which can only be modelled by accounting for non-linear wave loading effects. The most important are wave drift forces, springing, ringing and wave slam. The first two are very different in their physical manifestation, though their origin can be traced to a common theoretical

*Now at: W. S. Atkins, Berkshire House, 171 High Holborn, London WC1V 7AA, U. K.

model. It is found that both can be well explained by incorporating a first correction to linear theory: namely, the inclusion in a consistent manner of terms which depend on both linear and quadratic powers of wave elevation. Such a non-linear theory can be described as second order, and this forms the subject of this article.

Second order wave theory was first applied to modelling low frequency drift forces and responses. It is very clear that if an irregular wave elevation is modelled as a superposition of components at different frequencies, then quantities (*e.g.* forces and responses) proportional to the square of that elevation will contain terms at both the sums and differences of the elementary wave frequencies. It is the low (difference) frequency components which are found to excite the resonant response of floating platforms, such as semisubmersibles and floating production systems, in their horizontal modes (surge, sway and yaw); this is the phenomenon of wave drift responses. The related phenomenon at the sum frequencies is now generally known as springing. Arising at frequencies substantially higher than wave frequencies, springing becomes an important design issue on the context of lightly damped resonant responses in the "stiff" modes of certain types of offshore platform: notably the vertical modes (heave, pitch and roll) of Tension Leg Platforms (TLPs), and the cantilever modes of slender towers.

As second order effects can be demonstrated to be important in exciting resonant responses of stiff structures, one can imagine that higher order effects than second might also be relevant in certain circumstances. The phenomenon of "ringing" appears to be just such a case. When a steep-fronted wave encounters a large diameter vertical cylinder, it is found that high frequency load components are generated which cannot be adequately modelled by second order theory (either from the point of view of frequency content, or the nature of the statistics in random waves, which imply terms of at least cubic order in wave elevation). The effect of this wave-structure interaction has some similarities with an impulsive loading, and in a slender tower or TLP this can excite a sharp transient response similar to that resulting from an impact (hence the terminology, after "ringing" a bell). Slamming is more obviously an impulsive load effect, arising when a body accelerates through the air sea interface and its water plane area changes rapidly during the process. As such this is highly non-linear. To model slamming, and indeed the phenomenon of ringing, it seems necessary to undertake fully non-linear transient analyses, usually involving numerical time marching. The second order problems, however, are amenable to solution in the frequency domain, on the basis of the Stokes expansion technique. Where relevant, such solutions have several advantages over time domain analyses: computation of the hydrodynamic loading should be less expensive (and more reliable); and tools are available for both spectral

and probabilistic analyses of second order processes. It is these processes which form the subject of this article.

While the phenomena of springing and wave drift responses can both be modelled on the basis of second order hydrodynamic analysis and potential flow theory, there are of course very important differences in modelling them. The former is significantly more difficult than the latter, for two reasons. Firstly, it is found that at the difference frequencies relevant to wave drift excitation, the second order loading due to the second order velocity potential is generally very small in relation to the second order term arising from products of first order potential effects. Hence whereas the effect of the second order potential must be modelled in springing, it may generally be ignored in calculating wave drift forces (except in special cases such as shallow water). The evaluation of drift forces is then routine, as long as a reliable first order diffraction/radiation analysis is available (though the phenomenon of wave drift damping adds a degree of complexity to the analysis). Calculation of springing excitation, however, is not straightforward, because of the difficulty of evaluating the effects of the second order potential.

A second important difference in the second order modelling of wave drift and springing concerns the statistical treatment. Analytical expressions may be obtained for probability distributions and extreme value statistics of the second order low frequency processes. The treatment of second order sum frequency processes, however, is more complex.

In view of these differences, it is unrealistic to attempt to review both low frequency and high frequency second order phenomena within the compass of this article. We concentrate therefore on the high frequency springing problem, although of course a significant part of what is described below is also relevant to the wave drift phenomenon.

Further details on the phenomenon of springing, in the context of TLP design, have been given by Petrauskas & Liu (1987), Kim & Yue (1988), Eatock Taylor (1991), Marthinsen & Muren (1993), and Natvig (1993). The subject matter in the present article is arranged as follows. In the next section we review certain matters relating to the modelling of second order hydrodynamic effects in the frequency domain. This requires analysis in bichromatic waves (and, for modelling behaviour in spread seas, in bidirectional waves; but for simplicity we here restrict attention to behaviour in long-crested seas. The extension to two directions is algebraically more involved, but conceptually not much different). This review in section 2 includes both fully numerical treatment for bodies of arbitrary geometry; and semi-analytical solutions for various configurations of cylinders.

In section 3 we examine the spectral analysis of second order, non-linear processes. Analytical expressions are obtained for the spectra of simple

second order processes. These are used as benchmarks in illustrating the performance of discrete time simulation and associated FFT based spectral analysis of such processes. Finally, section 4 reviews the probabilistic treatment relevant to springing responses. This requires examination of processes which include both first and second order components. An extensive list of cited references is provided in each section to enable the reader to find further details of a subject which can only be treated at best superficially in what follows.

2 Second Order Hydrodynamics

2.1 *General formulation*

Tautly moored compliant offshore structures such as tension leg platforms are composed of large elements whose characteristic dimension, D, is typically large relative to the incident water wave length, L. If the incident wave height, H, is small relative to this characteristic dimension, such that $\frac{H}{D} < 1$, the motions of the water particles are small relative to the structure and the resulting drag forces developed are negligible. A discussion of the nature of wave loading under various flow régimes is given by Sarpkaya & Isaacson (1981). Inertial effects, proportional to the acceleration of the fluid, dominate the flow régime for this type of structure. Under these conditions the flow can be described in terms of a velocity potential and the incident and scattered or diffracted waves are expressed in terms of this potential. A mathematical formulation is presented for the problem of long crested incident waves interacting with a floating body. We use a Cartesian coordinate system in which the x-y plane is positioned at the level of the quiescent free surface with the z-axis pointing vertically upwards. The fluid domain, Ω, is bounded by the body surface, S_B, the free surface, S_F, the sea bed, S_S, and a boundary at infinity S_∞.

As the fluid is assumed to be in irrotational motion the flow can be described by a scalar velocity potential, $\Phi(x, y, z, t)$, which satisfies the Laplace equation in the domain, Ω

$$\nabla^2\Phi = \frac{\partial^2\Phi}{\partial x^2} + \frac{\partial^2\Phi}{\partial y^2} + \frac{\partial^2\Phi}{\partial z^2}. \tag{1}$$

Rigid, impermeable boundary conditions are applied on S_S, and S_B:

$$\frac{\partial\Phi}{\partial n} = 0, \tag{2}$$

where $\mathbf{n}$ is the unit normal to the surface. Two boundary conditions are applied over the free surface as neither the value of the potential, Φ, at the

surface nor the position of the free surface are known. If the equation of the free surface is defined as

$$z = \eta(x, y, t), \tag{3}$$

the dynamic boundary condition at the free surface is (*c.f.* Sarpkaya & Isaacson 1981 and Mei 1992)

$$\frac{\partial \Phi}{\partial t} + g\eta + \frac{1}{2}\left[\left(\frac{\partial \Phi}{\partial x}\right)^2 + \left(\frac{\partial \Phi}{\partial y}\right)^2 + \left(\frac{\partial \Phi}{\partial z}\right)^2\right] = 0 \tag{4}$$

which implies that the pressure is constant; and the kinematic boundary condition is

$$\frac{\partial \eta}{\partial t} + \frac{\partial \Phi}{\partial x}\frac{\partial \eta}{\partial x} + \frac{\partial \Phi}{\partial y}\frac{\partial \eta}{\partial y} - \frac{\partial \Phi}{\partial z} = 0. \tag{5}$$

Equations (4) and (5) are both applied at $z = \eta$. Finally, to ensure a physically realisable solution is obtained, a radiation condition must be imposed at the infinite boundary, S_∞, requiring that the scattered wave approach the form of a radially propagating wave at great distances from the body.

The pressure, p, at a point in the fluid can be found from Bernoulli's equation,

$$p = -\rho\left\{\frac{\partial \Phi}{\partial t} + g\eta + \frac{1}{2}\left[\left(\frac{\partial \Phi}{\partial x}\right)^2 + \left(\frac{\partial \Phi}{\partial y}\right)^2 + \left(\frac{\partial \Phi}{\partial z}\right)^2\right]\right\} \tag{6}$$

in which ρ is the fluid density.

As a result of the nonlinearities in the free surface condition, the velocity potential Φ can be expanded in a perturbation series in terms of the wave slope parameter, $\epsilon = \frac{H}{\lambda}$, where λ is the wave length and $\epsilon \ll 1$. Thus:

$$\Phi = \epsilon \Phi^{(1)} + \epsilon^2 \Phi^{(2)} + ... \tag{7}$$

The surface elevation, η, can similarly be written:

$$\eta = \epsilon \eta^{(1)} + \epsilon^2 \eta^{(2)} + \ldots . \tag{8}$$

The free surface boundary conditions are expanded in Taylor series about the mean position, $z = 0$, and equations (7) and (8) are substituted into the resulting expansions. Upon collection of like terms of the expansion parameter, ϵ, $(\epsilon(\cdot), \epsilon^2(\cdot), ...)$, the dynamic and kinematic free surface boundary conditions can be combined to eliminate $\eta^{(1)}$ and $\eta^{(2)}$. The first order combined free surface boundary condition at $z = 0$ is then

$$\frac{\partial^2 \Phi^{(1)}}{\partial t^2} + g\frac{\partial \Phi^{(1)}}{\partial z} = 0; \tag{9}$$

and the second order combined free surface condition is

$$\frac{\partial^2 \Phi^{(2)}}{\partial t^2} + g\frac{\partial \Phi^{(2)}}{\partial z} = \frac{1}{g}\frac{\partial \Phi^{(1)}}{\partial t}\left[\frac{\partial}{\partial z}\left(\frac{\partial^2 \Phi^{(1)}}{\partial t^2} + g\frac{\partial^2 \Phi^{(1)}}{\partial z^2}\right)\right] -$$

$$\frac{\partial}{\partial t}\left[\left(\frac{\partial \Phi^{(1)}}{\partial x}\right)^2 + \left(\frac{\partial \Phi^{(1)}}{\partial y}\right)^2 + \left(\frac{\partial \Phi^{(1)}}{\partial z}\right)^2\right], \qquad (10)$$

see Ogilvie (1983) for example. It may be noted that the free surface condition for $\Phi^{(2)}$ is inhomogeneous, and this causes considerable difficulties in developing solutions for the second order problem.

If the body is freely floating or able to move subject to some mooring restraint, it will undergo rigid body motions. In a general case the structure will have six degrees of freedom, three translational and three rotational, and each will generate a wave field which can be described by a velocity (radiation) potential. This problem is simplified at each order of analysis by assuming that the diffracted wave field can be computed from the incident waves interacting with a fixed body, and that the added mass and radiation damping effects due to the body motions can be decoupled from the incident wave field. Equation (7) can therefore be expressed in terms of incident (Φ_I), diffracted (Φ_D) and radiated potentials (Φ_R)

$$\Phi = \epsilon(\Phi_I^{(1)} + \Phi_D^{(1)} + \Phi_R^{(1)}) + \epsilon^2(\Phi_I^{(2)} + \Phi_D^{(2)} + \Phi_R^{(2)}) + \ldots \ . \qquad (11)$$

Here $\Phi_D^{(1)}$ describes the first order scattered waves due to the presence of the fixed body; and $\Phi_R^{(1)}$ represents the six wave systems generated by the body describing unit amplitude oscillations in the three translational and three rotational rigid body modes separately, in quiescent water (it is the sum of the six radiation potentials). The second order diffracted potential, $\Phi_D^{(2)}$, represents the scattering of the second order incident waves, in the presence of the inhomogeneous boundary condition on the free surface. The second order radiated potentials, $\Phi_R^{(2)}$, can be defined as representing the waves generated by the body as it describes second order motions in quiescent water subject to a homogeneous free surface condition.

We consider now the case when a body is placed in long crested bichromatic waves with frequencies ω_1, ω_2 and amplitudes A_1, A_2, in water of depth d. Bichromatic waves are considered, so that second order effects arising from wave components of different frequencies can be assessed. In particular, one can anticipate effects at $2\omega_1$, $2\omega_2$, $(\omega_1 + \omega_2)$, $(\omega_1 - \omega_2)$ and a mean component. For a bichromatic incident wave field the total first

order velocity potential can be decomposed in the form,

$$\Phi^{(1)}(\boldsymbol{x},t) = \Re\left\{\sum_{j=1}^{2}\phi_j^{(1)}(\boldsymbol{x})\,e^{-i\omega_j t}\right\}. \tag{12}$$

The second order velocity potential is the superposition of the sum and difference frequency terms

$$\Phi^{(2)}(\boldsymbol{x},t) = \Re\left\{\sum_{j=1}^{2}\sum_{l=1}^{2}\phi^{-}(\boldsymbol{x})\,e^{-i\omega^{-}t} + \phi^{+}(\boldsymbol{x})\,e^{-i\omega^{+}t}\right\} \tag{13}$$

where $\omega^{-} = \omega_j - \omega_l$ and $\omega^{+} = \omega_j + \omega_l$. The sum frequency potential, ϕ^{+}, includes double frequency components at $\omega^{+} = 2\omega_j, 2\omega_l$ and the component at the sum frequency, $\omega_j + \omega_l$. The difference frequency component is composed of terms at frequency $\omega_j - \omega_l$. The first order incident wave potential is written

$$\phi_{Ij}^{(1)} = \sum_{j=1}^{2}\frac{-igA_j}{\omega_j}\frac{\cosh k_j(z+d)}{\cosh k_j d}\exp(ik_j x) \tag{14}$$

where ω_j and the wave number, k_j, are related by the dispersion relationship

$$\omega_j^2 = gk_j\tanh(k_j d) \tag{15}$$

for $j = 1, 2$ and where g is the gravitational acceleration. The second order potential for bichromatic incident waves is given as (*e.g.* Bowers 1976)

$$\phi_I^{\pm}(r,\theta,z) = \frac{1}{2}(\alpha_{jl}^{\pm} + \beta_{lj}^{\pm})\frac{\cosh(k^{\pm}(z+h))}{\cosh k^{\pm}h}\exp(ik^{\pm}x), \tag{16}$$

where

$$\alpha_{jl}^{\pm} = \frac{-igA_j A_l}{2\omega_j}\frac{k_j^2(1-\tanh^2 k_j h) \pm 2k_j k_l(1 \mp \tanh k_j h \tanh k_l h)}{\nu^{\pm} - k^{\pm}\tanh k^{\pm}h}, \tag{17}$$

$$\beta_{lj}^{+} = \alpha_{lj}^{+}, \quad \beta_{lj}^{-} = \alpha_{lj}^{-*}, \quad k^{\pm} = k_j \pm k_l, \quad \nu^{\pm} = \omega^{\pm^2}/g.$$

The first order body disturbance potential, $\phi_B^{(1)}(=\phi_D^{(1)}+\phi_R^{(1)})$, in a wave of frequency ω_j, satisfies the following boundary conditions:

$$\frac{\partial\phi_{Bj}^{(1)}}{\partial n} = -\frac{\partial\phi_{Ij}^{(1)}}{\partial n} - i\omega_j\boldsymbol{n}\cdot(\boldsymbol{\xi}_j^{(1)} + \boldsymbol{\alpha}_j^{(1)}\times\boldsymbol{r}) \qquad \text{on } S_B, \tag{18}$$

$$-\omega_j^2 \phi_{Bj}^{(1)} + g\frac{\partial \phi_{Bj}^{(1)}}{\partial z} = 0 \qquad \text{on } S_F,\ z=0, \tag{19}$$

where $\boldsymbol{\alpha}_j^{(1)}=(\alpha_{xj}^{(1)},\alpha_{yj}^{(1)},\alpha_{zj}^{(1)})$ and $\boldsymbol{\xi}_j^{(1)}=(\xi_{xj}^{(1)},\xi_{yj}^{(1)},\xi_{zj}^{(1)})$ are the translational and rotational complex displacements (*i.e.* without the time factor $\exp(-i\omega_j t)$). The position vector on the body surface is denoted by the vector $\boldsymbol{r}$. A Sommerfeld radiation condition is also specified at the infinite boundary, S_∞

$$\lim_{R\to\infty} \sqrt{R}\left(\frac{\partial \phi_{Bj}^{(1)}}{\partial R} - ik_j \phi_{Bj}^{(1)}\right) = 0 \tag{20}$$

in which R is the radial distance from the origin.

The second order solution requires that the first order solution be available, in order to compute the inhomogeneous term of the free surface boundary condition on the right hand side of equation (10) and the forcing terms at second order. As sum frequency effects are the focus of this article, the second order boundary value problem is formulated in terms of the sum frequency potential, ϕ_D^+. The boundary conditions for this second order potential problem are

$$-\omega^{+^2}\phi_D^+ + g\frac{\partial \phi_D^+}{\partial z} = q^+ \qquad \text{on } S_F,\ z=0; \tag{21}$$

$$\frac{\partial \phi_D^+}{\partial z} = 0 \qquad \text{on } S_S; \tag{22}$$

$$\frac{\partial \phi_D^+}{\partial n} = -\frac{\partial \phi_I^+}{\partial n} + B^+ \qquad \text{on } S_B; \tag{23}$$

and a radiation condition at the infinite boundary, S_∞. Here S_B is now the mean position of the moving body, and B^+ is a second order forcing term associated with the motions of the body. The free surface forcing term, q^+, in equation (21) is written, *c.f.* Kim & Yue (1990),

$$q^+ = \frac{1}{2}(q_{jl}^+ + q_{lj}^+) \tag{24}$$

where

$$q_{jl}^+ = \frac{-i\omega_l}{2g}\phi_l^{(1)}\left(-\omega_j^2\frac{\partial \phi_j^{(1)}}{\partial z} + g\frac{\partial^2 \phi_j^{(1)}}{\partial z^2}\right) + i\omega_l \nabla\phi_j^{(1)}\cdot\nabla\phi_l^{(1)} - q_{IIjl}^+. \tag{25}$$

In this, q_{IIjl}^+ corresponds to the quadratic forcing term composed solely of incident wave potentials. The body forcing term, B^+, is similarly expressed as

$$B^+ = \frac{1}{2}(b_{jl}^+ + b_{lj}^+) \tag{26}$$

where

$$b_{jl}^{+} = \frac{1}{2}\boldsymbol{n} \cdot ((\boldsymbol{\xi}_l^{(1)} + \boldsymbol{\alpha}_l^{(1)} \times \boldsymbol{r}) \cdot \nabla)\nabla\phi_j^{(1)}. \tag{27}$$

The sum frequency second order radiation potentials, $\phi_R^{(2)}$, must satisfy a boundary condition on the body surface, similar to that in equation (18) without the incident wave term.

Once the velocity potentials have been obtained, the hydrodynamic forces acting on a body are found by integrating the pressure over the body surface

$$\boldsymbol{F} = \int\int_{S_B} p\boldsymbol{n}dS \tag{28}$$

where the pressure p is found from Bernoulli's equation (6). The first order force, $\boldsymbol{F}^{(1)}$, is found from

$$\boldsymbol{F}^{(1)} = -\rho \int\int_{S_B} \frac{\partial \Phi^{(1)}}{\partial t}\boldsymbol{n}dS. \tag{29}$$

The second order force, $\boldsymbol{F}^{(2)}$, is found, following Ogilvie (1983), from

$$\begin{aligned} \boldsymbol{F}^{(2)} = \quad & - \quad \rho\left[\int_{z=0} -\frac{g}{2}(\eta^{(1)})^2\boldsymbol{n}dl + \frac{1}{2}\int\int_{S_B}(\nabla\Phi^{(1)})^2\boldsymbol{n}dS\right. \\ & + \quad \left.\int\int_{S_B}\frac{\partial\Phi^{(2)}}{\partial t}\boldsymbol{n}dS\right] \end{aligned} \tag{30}$$

where $\int_{z=0} dl$ represents a line integral around the body at mean water level. The second order force acting on the body is composed of a term, $\boldsymbol{F}_Q^{(2)}$, involving quadratic components of the first order potentials as in the first two terms on the right hand side of equation (30); and a term due to the second order potential, $\boldsymbol{F}_P^{(2)}$. If the body is freely floating, a component, $\boldsymbol{F}_{BB}^{(2)}$, due to the motions is also found.

2.2 *Numerical solution*

2.2.1 *A boundary integral formulation*

The first and second order boundary value problems can be solved by boundary integral equations formulated by applying Green's theorem to the fluid domain. Such methods for solution of the first order diffraction/radiation problem are now widely used in industry. The second order problem is significantly more difficult to implement, and rather few attempts have been made. Examples may be found in the work of Chen

& Molin (1990), Matsui et al. (1990), Lee et al. (1991), Eatock Taylor & Chau (1992) and Lee & Newman (1994). In what follows we summarise the methodology adopted by Eatock Taylor & Chau (1992), which differs from most other work in two significant respects: quadratic rather than constant boundary elements are implemented; and a modified integral equation is used. Both of these features are aimed at improving the numerical efficiency of the calculation.

At first order, applying Green's theorem in the conventional way leads to

$$\begin{aligned} C(\boldsymbol{x}_0)\phi_{Bj}^{(1)}(\boldsymbol{x}_0) \quad &+ \quad \int\int_{S_B} \left(\phi_{Bj}^{(1)}(\boldsymbol{x}) \frac{\partial G_j}{\partial n} + G_j \frac{\partial \phi_{Ij}^{(1)}(\boldsymbol{x})}{\partial n} \right) dS \\ &= \quad \int\int_{S_B} G_j V_j^{(1)}(\boldsymbol{x}) dS \end{aligned} \tag{31}$$

in which, $\phi_{Bj}^{(1)}(\boldsymbol{x}_0)$, is the unknown disturbance potential due to the incident waves and a normal velocity $V_j^{(1)}(\boldsymbol{x})$ on the body surface. $G_j(\boldsymbol{x}, \boldsymbol{x}_0)$ is the Green function corresponding to an oscillating source at frequency ω_j. The function $C(\boldsymbol{x}_0)$ has the value 1 when $\boldsymbol{x}_0$ is in the fluid domain and $\frac{1}{2}$ if $\boldsymbol{x}_0$ is on S_B. The discontinuous behaviour of $C(\boldsymbol{x}_0)$ normal to the body surface can lead to difficulties in solving equation (31) near to the body and the integrand has a singularity associated with it. Chau & Eatock Taylor (1988) showed that this can be overcome by applying Green's theorem to the region interior to the body, $\Omega^{'}$, as suggested by Noblesse (1983). This leads to the modified integral equation

$$\begin{aligned} \phi_{Bj}^{(1)}(\boldsymbol{x}_0)[1 \quad &- \quad \nu_j \int\int_{S_{F'}} G_j dS] + \int\int_{S_B} \left([\phi_{Bj}^{(1)}(\boldsymbol{x}) - \phi_{Bj}^{(1)}(\boldsymbol{x}_0)] \frac{\partial G_j}{\partial n} \right. \\ &+ \quad \left. G_j \frac{\partial \phi_{Ij}^{(1)}(\boldsymbol{x})}{\partial n} \right) dS = \int\int_{S_B} G_j V_j^{(1)}(\boldsymbol{x}) dS. \end{aligned} \tag{32}$$

The intersection of the region interior to the body with the free surface is denoted by $S_{F'}$, and $\nu_j = \frac{\omega_j^2}{g}$. In this representation $C(\boldsymbol{x}_0)$ has been removed from the equation and the integrand is now non-singular, as shown by Chau (1989).

Solution of the sum frequency, second order boundary value problem for the velocity potential, ϕ_D^+, is achieved by again applying Green's identity to the fluid domain. This leads in a imilar way to

$$\phi_D^+(\boldsymbol{x}_0)(1 \quad - \quad \nu^+ \int\int_{S_{F'}} G^+ dS)$$

$$+ \quad \int\int_{S_B} \left\{ [\phi_D^+(\boldsymbol{x}) - \phi_D^+(\boldsymbol{x}_0)] \frac{\partial G^+}{\partial n} + G^+ \frac{\partial \phi_I^+(\boldsymbol{x})}{\partial n} \right\} dS$$

$$+ \quad \int\int_{S_F} q^+ G^+ dS = \int\int_{S_B} B^+ G^+ \, dS, \tag{33}$$

as shown by Eatock Taylor & Chau (1992). A corresponding equation for ϕ_R^+ may similarly be formulated, in which the free surface integral term in ϕ^+ is absent, and the right hand side is the second order equivalent of the right hand side of Eq. (32). It should be noted that the Green function appearing in both equations (32) and (33) satisfies the homogeneous boundary condition on the free surface: the only difference between them is that in the former case it corresponds to a wave source at ω_j while in the latter it is at the sum frequency ω^+.

Equations (32) and (33) are the foundations for determining a numerical solution to the hydrodynamic model of bichromatic potential flows described in this article. They have been implemented in a suite of computer programs called *DIFFRACT*. In the discretised models adopted in this boundary element solution, the body surface and internal water plane (and free surface for a second order analysis) are discretised into a number of panels or elements and the integrations are performed over each individually. An approximate form of the discretised integral equation is then derived as a sum of the contributions from each element. Collectively these form a linear algebraic set of equations which can be solved using well established matrix techniques. Elements of different order may be used in the analysis in which the function is assumed to be constant, or vary in some manner over the element. In *DIFFRACT* the variation of the geometry and the scattered potential over each element is modelled by 8-node quadrilateral, and 6-node triangular isoparametric quadratic elements. In this way, the potential or elemental geometry as defined in Cartesian space are mapped into a normalised local space associated with each element by the use of shape functions. Zienkiewicz (1977) describes the concepts and theory of isoparametric transformations. Use of the shape functions allows the potential at a general point in an element to be related to the nodal values of the potential. Quadratic boundary elements have the advantage over lower order elements as the variation of typical body geometries may often be described exactly. Panels in which a quantity is assumed to be constant lead to a discontinuous description of geometry of a curved body although with ever increasing computing power, more elements can be employed thereby reducing the effect of discontinuities. However, Liu *et al* (1990) suggest that for bodies with sharp corners, difficulties may be encountered when using a constant panel method.

In *DIFFRACT* the integration over each element in the normalised local

space is performed by two-dimensional, 4-point Gaussian quadrature. Chau (1989) notes that lower order derivatives in the integrand may still contain some singularities, and describes a triangular polar coordinate transformation which has the effect of concentrating the integration points around the singular node.

In the second order analysis, it can be seen that the problem as defined in equation (33) requires the evaluation of an integral over the entire free surface. The integrand, q^+G^+, involves the products of derivatives of the first order potential and is highly oscillatory. Furthermore, it may be shown that it only decays algebraically with increasing distance from the body. Clearly truncation of this integral near to the body may introduce errors into the analysis, so it is convenient to divide the free surface into three regions over which the integral is treated entirely differently. In the immediate vicinity of the body the integral can be evaluated numerically, *e.g.* using quadratic elements. A far-field region can be defined in which all of the evanescent, local, components of the scattered wave are assumed to have died away and all that remains is a radially propagating wave. In this region the scattered potential can be approximated by an asymptotic expansion. An adaptive middle region can then be defined, extending from the outer limit of the region of numerical quadrature, and in which are included a finite number of evanescent modes. The extent of this region can be calculated adaptively by comparing the value computed at its outer limit with the value computed at that position from the asymptotic analysis.

2.2.2 *Convergence of the higher order boundary element formulation*

In the boundary element approach, the homogeneous free surface condition is strictly satisfied by the Green function; the inhomogeneous free surface condition is satisfied by means of the free surface integral; and the body surface mesh determines the accuracy in satisfying the boundary condition on the body surface. Convergence of the method will depend crucially on the adequacy of the discretisation on these surfaces, the accuracy of the numerical integrations, and the number of terms in the series representing the far field behaviour. The second order problem is the more critical, because of the difficult free surface integral and its dependence on the discretised solution of the first order potentials.

We first illustrate the convergence characteristics of the first order solution, distinguishing between two aspects which determine the required fineness of the the body-surface mesh: (1) the first order total force calculation; (2) the first order potential calculation at some representative points on the free-surface. It is the latter which will influence the reliability of the free surface integral in the second order analysis. Several examples are now

Table 1: Effect of circumferential mesh number on accuracy of computation of non-dimensional horizontal force $|\hat{F}_x^{(1)}|$

	ka	0.10	0.40	0.80	1.20	1.60	2.00
$\|\hat{F}_x^{(1)}\|$	$N_c = 1$	0.6130	1.5618	1.5615	1.1118	0.7833	0.5898
	$N_c = 2$	0.6290	1.6016	1.5818	1.1100	0.7685	0.5600
	$N_c = 3$	0.6300	1.6039	1.5827	1.1103	0.7688	0.5603
	$N_c = 4$	0.6307	1.6045	1.5831			
	Analytical	0.6311	1.6057	1.5834	1.1106	0.7689	0.5604

Table 2: Effect of circumferential mesh number on accuracy of computation of non-dimensional vertical force $|\hat{F}_z^{(1)}|$

	ka	0.10	0.40	0.80
$\|\hat{F}_z^{(1)}\|$	$N_c = 1$	0.6337	0.1480	0.0225
	$N_c = 2$	0.6398	0.1487	0.0225
	$N_c = 3$	0.6402	0.1488	0.0225
	Analytical	0.6397	0.1482	0.0223

given, based on quadratic boundary elements, to illustrate the influence of the body surface mesh on the convergence. The structure examined is a fixed truncated vertical cylinder of radius a, draught $b = 4a$ and in water of depth $d = 20a$. The attraction of this example is that, for both first and second order problems, analytical solutions are available for comparison with the numerical results (see below, and Huang & Eatock Taylor 1996).

Example 2.1 *Influence of mesh density on the first order force calculation*

We define the total non-dimensional surge and heave forces in a wave of amplitude A, after factoring the time dependence, as

$$\hat{F}_x^{(1)} = \frac{F_x^{(1)}}{\pi\rho g a^2 A}, \quad \hat{F}_z^{(1)} = \frac{F_z^{(1)}}{\pi\rho g a^2 A}$$

. We use the notations N_c and N_z to represent circumferential and vertical numbers of elements in one quadrant of the cylinder surface. Tables 1 and 2 concern the convergence characteristics when N_c is varied, while N_z is kept as $N_z = 4$; results for the non-dimensional surge and heave forces are given over a range of wave numbers. These demonstrate that $N_c \leq 3$ gives satisfactory results for the first order force calculations in this case.

Table 3: Effect of vertical mesh number on accuracy of computation of non-dimensional horizontal force $|\hat{F}_x^{(1)}|$

	ka	0.10	0.40	0.80	1.20	1.60	2.00
$\|\hat{F}_x^{(1)}\|$	$N_z = 2$	0.6269	1.6010	1.5851	1.1111	0.7691	0.5592
	$N_z = 3$	0.6290	1.6029	1.5833	1.1105	0.7688	0.5601
	$N_z = 4$	0.6300	1.6039	1.5827			
	Analytical	0.6311	1.6057	1.5834	1.1106	0.7689	0.5605

Table 4: Effect of vertical mesh number on accuracy of computation of non-dimensional vertical force $|\hat{F}_z^{(1)}|$

	ka	0.10	0.40	0.80	1.20
$\|\hat{F}_z^{(1)}\|$	$N_z = 2$	0.6414	0.1500	0.0228	0.0038
	$N_z = 3$	0.6408	0.1494	0.0226	0.0036
	Analytical	0.6397	0.1482	0.0223	0.0035

Table 5: Convergence characteristics of the vertical mesh for $b/a = 8$

	ka	0.20	0.40	0.80	1.20	1.40
$\|\hat{F}_x^{(1)}\|$	$N_z = 3$	1.6064	1.9587	1.6606	1.1127	0.9241
	$N_z = 4$	1.6123	1.9624	1.6586	1.1219	0.9233
$\|\hat{F}_z^{(1)}\| \times 10^3$	$N_z = 3$	176.70	30.254	0.9232	0.0501	0.0317
	$N_z = 4$	176.40	30.172	0.9243	0.0506	0.0320

The influence of the vertical mesh on the force calculation is shown in tables 3 and 4. The circumferential mesh number is kept at $N_c = 3$.

Example 2.2 *Influence of draught b/a on the convergence characteristics of the vertical mesh*

A deeper draught body, of $b/a = 8$, is now considered. The circumferential mesh is fixed at $N_c = 3$. The calculated horizontal and vertical forces for two different vertical meshes are listed in table 5. This indicates that even for this deep draught , $N_z = 4$ is sufficient to obtain an accuracy of 99 % over this range of frequencies.

Table 6: Convergence of body surface mesh in calculating the first order potential on the free surface

	r/a	1.0	2.0	4.0	8.0	12.0
Re	mesh 1	-15.8019	-11.0654	11.0741	-11.3672	5.3137
	mesh 2	-15.8609	-11.1717	11.0502	-11.3878	5.3137
	mesh 3	-15.9370	-11.1760	11.0501	-11.3893	5.3137
	mesh 4	-15.9137	-11.1764	11.0501	-11.3895	5.3137
	Analytical	-15.9219	-11.1774	11.0501	-11.3895	5.3137
Im	mesh 1	-5.9881	-0.5231	6.6046	-0.5684	-8.3567
	mesh 2	-5.8963	-0.4787	6.5497	-0.5323	-8.3567
	mesh 3	-5.9102	-0.4767	6.5466	-0.5306	-8.3567
	mesh 4	-5.9030	-0.4764	6.5463	-0.5305	-8.3567
	Analytical	-5.9080	-0.4762	6.5463	-0.5304	-8.3567

Example 2.3 *Effect of body mesh on the diffraction potential on the free-surface*

As discussed above, in relation to obtaining second order results a more convincing test of the convergence characteristics of the body surface mesh would be to compare the results for the first order potential on the free surface. Table 6 gives a comparison of this potential at five points on the free surface at $\theta = \pi$ (*i.e.* the upwave side), $r/a = 1, 2, 4, 8, 12$ for four different body meshes on a truncated cylinder with draught $b = 2a$, in water of depth $d = 20a$, at dimensionless wave number $ka = 1.0$. (The potential tabulated is in fact dimensional, based on $a = 10$m). The different body meshes are: mesh 1, $N_c \times N_z = 2 \times 2$; mesh 2, $N_c \times N_z = 3 \times 3$; mesh 3, $N_c \times N_z = 4 \times 4$; and mesh 4, $N_c \times N_z = 5 \times 5$. In each case the number of elements radially on the bottom of the cylinder, N_b, was equal to N_c. The analytical solution is also listed for comparison. One can see that the largest error in the calculation of the potential using the boundary element simulation occurs on the body surface. Even a fairly coarse mesh can produce an acceptable accuracy for potentials at $r/a \geq 2$. For a high accuracy on the body surface, a relatively fine mesh is required. In the present case, a 3×3 body mesh (mesh 2) yields a satisfactory accuracy. This is consistent with the previous analysis for the force calculations.

Example 2.4 *Influence of the outer radius of the free surface mesh on convergence of the second order force calculations*

Solution of the second order problem involves the free surface integral, which is calculated by two dimensional quadrature in an inner domain bounded externally by a circle of radius R_J. Outside that domain the integral is expressed as a Fourier series, and the circumferential integration is performed in closed form. The value of the outer radius R_J, and the discretisation within it, are clearly likely to have important influences on the accuracy of the second order results. We illustrate this by examining results for second order forces on a truncated cylinder. The time-independent sum frequency forces are non-dimensionalised as:

$$\hat{F}_x^+ = \frac{F_x^+}{\rho g a A_1 A_2}, \quad \hat{F}_z^+ = \frac{F_z^+}{\rho g a A_1 A_2}.$$

We use R_J/d as the parameter for examining the convergence characteristics, in considering a truncated cylinder of $b/a = 3$, $d/a = 10$ in a monochromatic wave field. The second order surge and heave forces, for different R_J/d, are listed in tables 7 and 8 for three dimensionless wave numbers. The body mesh in one quadrant was defined by: $N_c \times N_z \times N_b = 4 \times 4 \times 4$; and the free surface meshes in one quadrant corresponded to: $N_c \times N_r = 6 \times 5$ for $R_J/d = 2$; 6×10 for $R_J/d = 3$; and 6×15 for $R_J/d = 4$. (N_r is the number of elements radially on the free surface; N_c is the number of elements circumferentially on both the body and the free surface).

The conclusion to be drawn from these and many other results in an extensive convergence study is that the linear and second order calculations have rather different requirements in terms of the boundary element discretisation. This is perhaps not surprising. For linear (first order and homogeneous part of second order) analysis, even a very coarse mesh on the body surface can yield suprisingly high accuracy. The second order analysis is, on the other hand, very sensitive to the mesh on both the body surface and free surface, and insufficient mesh density may result in substantial computational errors.

2.3 *Semi-analytical solutions for fixed vertical cylinders*

Although many numerical investigations have been carried out for second order wave diffraction problems, complete semi-analytical solutions, which are capable of calculating both hydrodynamic forces and free surface elevations, are desirable. These can serve the following purposes:

Table 7: Influence of R_J/d on convergence of second order surge force for a truncated cylinder with $b/a = 3$

ka	1.0		1.4		1.6	
R_J/d	Re	Im	Re	Im	Re	Im
2.0	0.8641	0.4927	1.9794	0.4926	2.4590	−0.5792
3.0	0.8674	0.4935	1.9811	0.4964	2.4631	−0.5798
4.0	0.8681	0.4939	1.9826	0.4978	2.4652	−0.5804
Analytical	0.8683	0.4944	1.9828	0.4984	2.4670	−0.5808

Table 8: Influence of R_J/d on convergence of second order heave force for a truncated cylinder with $b/a = 3$

ka	1.0		1.4		1.6	
R_J/d	Re	Im	Re	Im	Re	Im
2.0	−0.0082	−0.4980	−0.2148	−0.2301	−0.5341	0.1372
3.0	−0.0079	−0.4981	−0.2151	−0.2305	−0.5344	0.1378
4.0	−0.0079	−0.4981	−0.2151	−0.2305	−0.5344	0.1378
Analytical	−0.0078	−0.4982	−0.2153	−0.2304	−0.5347	0.1379

- To provide a tool to check the accuracy and convergence of the numerical calculations.
- To gain a better understanding of the physical nature of the second order wave-structure interaction problem.
- To provide an efficient algorithm for fast evaluation of the second order wave loads on TLPs, by combining with the boundary element method.

The first reliable semi-analytical solutions for second order diffraction forces were based on an indirect formulation proposed independently by Lighthill (1979) and Molin (1979). In this, a reciprocal theorem (in effect Green's identity) is used to express the force by integration of products of first order quantities, thereby avoiding explicit determination of the second order potential. This indirect method has been used to compute second order loads on a single vertical cylinder (Eatock Taylor & Hung 1987) and arrays of vertical cylinders in monochromatic waves (Ghalayini & Williams 1991) and in bichromatic waves (Moubayed & Williams 1995). The implementation of the single cylinder formulation was improved by Newman (1996) through use of the Weber transform, leading to results in agreement with those of Eatock Taylor & Hung (1987).

The disadvantage of the indirect method is that it does not readily provide the second order wave elevation and kinematics. This problem was addressed by Chau & Eatock Taylor (1992) and Kriebel (1992), who independently obtained semi-analytical expressions for the second order potential itself, associated with diffraction of regular waves by a vertical cylinder. Results could then be obtained for such quantities as the second order run-up around the cylinder. Teng & Kato (1995) sought an improved method of computing the second order potential, based on the same basic idea. Huang & Eatock Taylor (1996) extended the direct formulation to obtain semi-analytical expressions for the second order potential in the case of a truncated cylinder in regular waves; and Eatock Taylor & Huang (1997a) showed how this could be used in combination with a numerical near-field approach to solve the analogous problem for an arbitrary axisymmetric body in monochromatic waves. The extension of the semi-analytical direct formulation to bichromatic waves was given by Eatock Taylor & Huang (1997b).

Application of the direct solution method to obtain the second order potential around groups of vertical cylinders is rather less straightforward (Huang & Eatock Taylor 1997, Malenica 1997). A summary of the approach is presented here for the bichromatic wave case. The starting point is the exact interaction theory of Linton & Evans (1990) for the first order potentials. The free surface integrals are performed in terms of local polar coordinate systems which coincide with the individual cylinders, and are transformed into one dimension by using the Fourier expansion method.

We consider therefore the diffraction of a plane bichromatic wave by a group of vertical circular cylinders of radius a and draught b. As before, we decompose the first and second order velocity potentials as follows:

$$\phi_j^{(1)} = \phi_{Ij}^{(1)} + \phi_{Dj}^{(1)}, \quad \phi^+ = \phi_I^+ + \phi_D^+. \tag{34}$$

We divide the fluid domain into two parts: an exterior region which is defined as the region outside the cylinders when they are extended to the seabed; and an "interior" region consisting of N_c sub-regions (N_c being the number of cylinders), with the kth sub-region defined by:

$$(x - x_{ck})^2 + (y - y_{ck})^2 \leq a^2; \ -d \leq z \leq -b.$$

(x_{ck}, y_{ck}) are the horizontal coordinates of the axis of the kth cylinder.

In the exterior region, we express the velocity potentials in terms of local coordinate systems (r_k, θ_k, z), using an approach similar to that of

Linton & Evans (1990):

$$\phi_{Ij}^{(1)} = C_k \sum_{n=-\infty}^{\infty} J_n(k_j r_k) e^{in(\pi/2-\beta)} e^{in\theta_k} f_0(z),\ C_k = e^{ik_j(x_{ck}\cos\beta + y_{ck}\sin\beta)} \tag{35}$$

where k_j is the first order wavenumber corresponding to wave frequency ω_j; β is the angle of incidence of the wave; and

$$\phi_{Dj}^{(1)} = \sum_{n=-\infty}^{\infty} \sum_{s=1}^{N_c} \{A_{j,n}^s \frac{H_n(k_j r_s)}{H_n'(k_j a)} f_j(z) + \sum_{m=0}^{\infty} B_{j,nm}^s \frac{U_n(k_{jm} r_s)}{U_n'(k_{jm} a)} Z_{jm}^{(1)}(z)\} e^{in\theta_s} \tag{36}$$

where

$$f_j(z) = \frac{\cosh(k_j(z+d))}{\cosh k_j d}, \tag{37}$$

$$U_n(k_{jm} r) = \begin{cases} H_n(k_j r) & m = 0 \\ K_n(k_{jm} r) & m > 0, \end{cases} \tag{38}$$

and

$$Z_{j0}^{(1)}(z) = \frac{1}{\sqrt{N_0}} \cosh(k_j(z+d)), \qquad N_0 = \frac{d}{2}(1 + \frac{\sinh(2k_j d)}{2k_j d}) \tag{39}$$

$$Z_{jm}^{(1)}(z) = \frac{1}{\sqrt{N_m}} \cos(k_{jm}(z+d)) \qquad N_m = \frac{d}{2}(1 + \frac{\sin(2k_{jm} d)}{2k_{jm} d}), \qquad m > 0. \tag{40}$$

k_j, k_{jm} $(m = 1, 2, \cdots)$ are the real roots of the corresponding dispersion equations:

$$k_j \tanh(k_j d) = \nu_j, \quad k_m \tan(k_{jm} d) = -\nu_j.$$

$A_{j,n}^s$ are the coefficients corresponding to the first order wave diffraction by multiple bottom-seated cylinders, and $B_{j,nm}$ are the coefficients taking into account the truncation of the cylinders (we restrict our analysis here to cylinders with the same size and the same draught).

The first order diffraction potential in the vicinity of cylinder k can be expressed in terms of the coordinate system (r_k, θ_k, z), based on Graf's addition theorem for Bessel functions:

$$X_m(\kappa r_s) e^{im\theta_s} = \sum_{n=-\infty}^{\infty} X_{m-n}(\kappa R_{ks}) e^{i(m-n)(\alpha_{jk}-\pi)} J_n(\kappa r_k) e^{in\theta_k}, r_k < R_{ks} \tag{41}$$

$$X_m(\kappa r_s)e^{im\theta_s} = \sum_{n=-\infty}^{\infty} J_{m-n}(\kappa R_{ks})e^{i(m-n)(\alpha_{jk}-\pi)}X_n(\kappa r_k)e^{in\theta_k}, r_k > R_{ks} \tag{42}$$

where κ is a wave number and $X_m(x)$ denotes $H_m(x), K_m(x)$ or $J_m(x)$ according to the circumstances. R_{ks} is the length of the vector joining the centres of cylinders k and s, and α_{ks} is its angle to the x axis.

Upon using the addition theorem, $\phi_{Dj}^{(1)}$ can be expressed as:

$$\begin{aligned}\phi_{Dj}^{(1)} &= \sum_{m=-\infty}^{\infty}\sum_{s=1}^{N_c}\{\sum_{n=-\infty}^{\infty}[A_{j,n}^s \frac{H_{n-m}(k_j R_{ks})}{H_n'(k_j a)}J_m(k_j r_k)f_j(z) + \\ &\quad \sum_{q=0}^{\infty} B_{j,nq}^s \frac{U_{n-m}(k_{jq}R_{ks})}{U_n'(k_{jm}a)}Z_{jq}^{(1)}(z)I_m(k_{jq}r_k)]e^{i(n-m)(\alpha_{ks}-\pi)}]\}e^{im\theta_k}, \\ &\quad r < R_{ks}. \end{aligned} \tag{43}$$

As stated above, the coefficients $A_{j,n}^s$ correspond to the first order diffraction of waves by bottom-seated cylinders, with the boundary condition at $r_k = a$:

$$\frac{\partial \phi_D^{(1)}}{\partial r_k}|_{r_k=a} = -\frac{\partial \phi_I^{(1)}}{\partial r_k}|_{r_k=a}, \ -d \le z \le 0.$$

This condition leads to the following expression for $A_{j,n}^s$:

$$\begin{aligned} A_{jm}^k &+ \sum_{s=1,s\neq k}^{N_c}\sum_{n=-\infty}^{\infty} A_{jn}^s \frac{H_{n-m}(k_j R_{ks})}{H_n'(k_j a)}J_m'(k_j a)e^{i(n-m)\alpha_{ks}}\delta_{ks} \\ &= -C_k e^{im(\pi/2-\beta)}J_m'(k_j a). \end{aligned} \tag{44}$$

The coefficients $B_{j,mn}^k$ are determined using the continuity condition for the normal velocity on the interface of the interior-exterior regions:

$$(\frac{\partial \phi_{D1}^{(1)}}{\partial r_k} + \frac{\partial \phi_{D2}^{(1)}}{\partial r_k} + \frac{\partial \phi_I^{(1)}}{\partial r_k})|_{r_k=a} = \begin{cases} 0 & -b \le z \le 0 \\ \frac{\partial \phi_{kj}^{(1)}}{\partial r_k}|_{r_k=a} & -d \le z \le -b \end{cases} \tag{45}$$

where $\phi_{D1}^{(1)}$ is the diffraction potential corresponding to a group of bottom-seated cylinders, $\phi_{D2}^{(1)}$ is the correction term due to the truncation of the cylinders, and $\phi_{kj}^{(1)}$ is the first order potential in the kth interior region.

Inside the kth interior region, the velocity potential can be expressed as:

$$\phi_{kj}^{(1)}(r_k,\theta_k,z)=\sum_{m=-\infty}^{\infty}\sum_{q=-\infty}^{\infty}\beta_{j,mq}^{k}V_m(\lambda_q r_k)\cos\lambda_q(z+h)e^{im\theta_k} \tag{46}$$

where

$$V_m(\lambda_q r)=\begin{cases}0.5(r/a)^m & q=0\\ I_m(\lambda_q r)/I_m(\lambda_q a) & q>0\end{cases} \tag{47}$$

with

$$\lambda_q=q\pi/d. \tag{48}$$

I_m is the mth modified Bessel function of the first kind. By applying the continuity equation for the normal velocity on the kth interface, involving the use of orthogonality of the eigenfunctions, we can derive the following expression for the unknown coefficients $B_{j,mn}^{k}$ in equation (43):

$$\begin{aligned}B_{j,mq}^{k} \quad &+ \quad \sum_{s=1,s\neq k}^{N_c}\sum_{n=-\infty}^{\infty}B_{j,nq}^{s}\frac{H_{n-m}(k_{jq}R_{ks})}{H_n'(k_{jq}a)}J_m'(k_{jq}a)e^{i(n-m)\alpha_{ks}}\delta_{ks}\\ &= \quad g_j(k,m,q)\end{aligned} \tag{49}$$

where

$$\alpha_{ks},\delta_{ks}=\begin{cases}\tan^{-1}[(y_{ck}-y_{cs})/(x_{ck}-x_{cs})], & 1 & x_{ck}>x_{cs}\\ -\tan^{-1}[(y_{ck}-y_{cs})/(x_{ck}-x_{cs})], & (-1)^{m-n} & x_{ck}<x_{cs}\end{cases}$$

$$g_j(k,m,q)=\int_{-d}^{-b}\sum_{p=0}^{\infty}\beta_{j,mp}^{k}V_m'(\lambda_p a)\cos\lambda_p(z+d)Z_{jq}^{(1)}(z)/k_{jq}dz.$$

The coefficients $\beta_{j,mq}^{k}$ in equation (46) can be determined using the potential continuity condition on the interfaces between the regions. This leads to:

$$\beta_{j,mq}^{k}V_m(\lambda_q a)=\frac{d}{2}\int_{-d}^{-b}[\phi_{Im}^{(1)}(a,z)+\phi_{Dm}^{(1)}(a,z)]\cos\lambda_q(z+d)dz \tag{50}$$

where $\phi_{Im}^{(1)}(a,z)$ and $\phi_{Dm}^{(1)}(a,z)$ are respectively the mth Fourier mode of the incident and diffraction potentials in the exterior region on the kth interface. For bottom-seated cylinders, the terms corresponding to the evanescent waves will vanish, and we only need to consider the terms associated with the coefficients A_{jm}^{k}.

The second order diffraction potential in the exterior region is decomposed into three parts:

$$\phi_D^+(x,y,z) = \phi_{D1}^+(x,y,z) + \phi_{D2}^+(x,y,z) + \phi_{D3}^+(x,y,z). \tag{51}$$

ϕ_{D1}^+ and ϕ_{D3}^+ satisfy the homogeneous free surface condition, Eq. (21) with $q^+ = 0$. ϕ_{D2}^+, the locked wave potential, satisfies the full inhomogeneous free surface condition. At the interfaces between the interior and exterior regions, the following conditions are specified for the three components:

$$\frac{\partial \phi_{D1}^+}{\partial r_k} = -\frac{\partial \phi_I^+}{\partial r_k}, \text{ at } r_k = a, -d \le z \le 0; \tag{52}$$

$$\frac{\partial \phi_{D2}^+}{\partial r_k} = 0 \text{ at } r_k = a, -d \le z \le 0; \tag{53}$$

$$\frac{\partial \phi_{D3}^+}{\partial r_k} = \begin{cases} 0, & r_k = a \quad -b \le z \le 0 \\ \partial \phi_k^+ / \partial r_k, & r_k = a \quad -d \le z \le -b \end{cases} \tag{54}$$

$$\phi_{D3}^+(a,\theta,z) = \phi_k^+(a,\theta,z), \quad -d \le z \le -b. \tag{55}$$

Here ϕ_k^+ is the second order potential in the interior region below the kth truncated cylinder.

The solution for ϕ_{D1}^+ may be obtained in a straightforward manner, in the same way as for the linear free wave diffracted by a fixed cylinder extending to the seabed. The procedure for obtaining the solution to the second order diffracted potential ϕ_{D2}^+, which satisfies the inhomogeneous boundary condition, is the same for both bottom-seated and fixed truncated cylinders. Based on Green's second identity, ϕ_{D2}^+ can be expressed as:

$$\phi_{D2}^+(r_k, \theta_k, z) = \frac{1}{2\pi} \int \int_{S_F} q^+(s) G^+(r_k, \theta_k, z; s) ds, \tag{56}$$

where S_F is the entire quiescent free surface excluding the cross-sections of the cylinders where they intersect the free surface. We now expand both $q^+(\rho_k, \theta_k)$ and $G^+(r_k, \theta_k, z; \rho_k, \theta_k)$ into Fourier components, and apply an eigenfunction expansion in z. We have:

$$q^+(\rho_k, \theta_k) = \sum_{m=-\infty}^{\infty} q_m^+(\rho_k) e^{im\theta_k}, \tag{57}$$

and

$$G^+(r_k, \theta_k, z; \rho_k, \theta_k', 0) = \sum_{m=-\infty}^{\infty} \sum_{n=0}^{\infty} G_{mn}^+(r_k, z; \rho_k, 0) e^{im(\theta_k - \theta_k')}; \tag{58}$$

where for $\rho_k > r_k$

$$G^+_{mn}(r_k, z; \rho_k, 0) = \begin{cases} \frac{\pi}{2} J_m(k_0^+ r_k) Z_0^+(k_0^+ z) Z_0^+(0) H_m(k_0^+ \rho_k) & n = 0 \\ I_m(k_0^+ r_k) Z_0^+(k_0^+ z) Z_0^+(0) K_m(k_0^+ \rho_k) & n > 0, \end{cases} \tag{59}$$

and for $\rho_k \leq r_k$

$$G^+_{mn}(r_k, z; \rho_k, 0) = \begin{cases} \frac{\pi}{2} J_m(k_n^+ \rho_k) Z_0^+(k_n^+ z) Z_0^+(0) H_m(k_n^+ r_k) & n = 0 \\ I_m(k_n^+ \rho_k) Z_0^+(k_n^+ z) Z_0^+(0) K_m(k_n^+ r_k) & n > 0. \end{cases} \tag{60}$$

The vertical eigenfunctions for the second order problem are defined similarly to the first order equivalents in Eq. (39) and (40), and the wave numbers k_0^+ and k_m^+ are real roots of the dispersion equations:

$$k_0^+ \tanh k_0^+ d = \nu^+, \quad k_m^+ \tan(k_m^+ d) = -\nu^+. \tag{61}$$

Integrating with respect to θ'_k, we can reduce the two-dimensional free surface integral into one dimension. This leads to:

$$\phi^+_{D2}(r_k, \theta_k, z) = \sum_{n=-\infty}^{\infty} e^{in\theta_k} \{ \sum_{m=0}^{\infty} Z_m^+(0) Z_m^+(z) \int_{a_k}^{\infty} \xi q_n^+(\xi) G^+_{mn}(r_k, \xi) d\xi \}. \tag{62}$$

Finally we consider the free wave component ϕ^+_{D3} in the exterior region, and the total second order potential ϕ_k^+ in the kth interior region. An appropriate form for this second order free wave component, satisfying the homogeneous boundary condition on the free surface, is:

$$\phi^+_{D3} = \sum_{l=1}^{N_c} \sum_{n=-\infty}^{\infty} \sum_{q=0}^{\infty} C^l_{nq} U_n(\kappa_q^+ r_l) Z_q^+(z) e^{in\theta_l}. \tag{63}$$

This also satisfies appropriate conditions at $r_k = a$, obtained from Eq. (54). The procedure for obtaining the coefficients by exploiting the orthogonality of the vertical eigenfunctions is similar to that employed for the first order problem in Eq. (49).

The most challenging part of the analysis concerns the evaluation of the free surface integral in the expression for ϕ^+_{D2}, Eq. (62). One possible approach is as follows (Huang & Eatock Taylor 1997). The intervals of the free surface integrals, in terms of the kth local polar coordinate system, are divided into three parts: the near-field region $r_k < R_{min}$ (where $R_{min} = min\{R_{jk}\}, \quad j, k = 1, 2, \cdots N_c$); the intermediate part, and the far-field part. In the near-field region, the free surface forcing function q_n^+ possesses a simple form, due to the simple expression for $\phi_j^{(1)}$, resulting from the

Table 9 Comparison of forces (N) for two bottom-seated cylinders, separated downwave by a distance $2a$ ($a = 1m, A = 1m$), in two water depths. First row: boundary element results from *DIFFRACT*; second row: semi-analytical results

	Total 1st order force		2nd order potential force	
d/a	$ka = 0.5$	$ka = 1.4$	$ka = 0.5$	$ka = 1.4$
1	2.579E+4	5.355E+4	6.817E+4	2.689E+4
	2.566E+4	5.327E+4	6.626E+4	2.726E+4
3	5.052E+4	6.046E+4	2.503E+4	6.457E+4
	5.026E+4	6.034E+4	2.423E+4	6.583E+4

addition theorem of Bessel functions. This form, however, is not valid in the intermediate and far-field regions. For the intermediate region, one can use a Fourier expansion in the circumferential direction and an interpolation in the radial direction to separate the variables (r, θ) in the forcing functions. In the far-field region, the local evanescent terms in the velocity potentials can be neglected, and the free-surface integrals performed analytically (Kim & Yue 1989, Eatock Taylor & Chau 1992).

To illustrate the semi-analytical solution, we compare the results it gives with those produced by the computer program *DIFFRACT*. We consider a configuration of two cylinders separated by a distance $4a$ in the direction of wave propagation. Results for this case were given by Chau (1989). Table 9 shows a comparison of results for the first and second order horizontal forces ($F_x^{(1)}$ and $F_{Px}^{(2)}$) from the semi-analytical and numerical methods, for two frequencies (as represented by ka) and two water depths. The agreement is seen to be satisfactory.

2.4 *Concluding remarks*

Second order analyses of even simple structures show that the forces are highly sensitive to the frequencies of the wave components. This implies that in order to achieve a satisfactory accuracy for second order wave loads in irregular waves, the calculations need to be done for a large number of frequency pairs. This is especially crucial for multi-column structures such as TLPs, where the interactions between columns lead to very rapid variations with frequency. Furthermore, it has been shown (e.g. Chen *et al.* 1991, Kim 1991) that the pontoons of a TLP make a significant contribution to second order diffraction. This effect can not be neglected, especially for heave, pitch and roll excitations. This makes the second order analysis of TLPs a heavy computational burden. Fortunately, for springing analysis

in the wave frequency band of practical interest, the lower part of the TLP, namely the pontoons, does not make much contribution to the first order diffracted potentials on the free surface. This suggests an efficient way of combining the semi-analytical and numerical solutions. The multi-column analytical theory can be used to obtain the first order potentials on the free surface, based on which one can obtain the particular solution of the second order potential (the locked wave component, ϕ_{D2}^{+}). The locked wave potentials on the body surface can thus be evaluated efficiently by using the semi-analytical solutions. Once these are known, the free wave component and the subsequent second order wave forces can be obtained using the standard boundary element numerical approach.

3 Spectra of Second Order Processes

3.1 *Volterra series representation*

We now consider an input-output system characterising linear plus second order forcing and response of offshore structures in random waves, based on the assumption that the second order forces in bichromatic waves can be obtained using methods such as described in the previous section. The response of the second-order system, $y(t)$, to an input function, $x(t)$, can be represented by the functional expansion (Schetzen, 1980):

$$y(t) = \int_{-\infty}^{\infty} h_1(\tau)x(t-\tau)d\tau + \int_{-\infty}^{\infty}\int_{-\infty}^{\infty} h_2(\tau,\tau')x(t-\tau)x(t-\tau')d\tau d\tau' \tag{64}$$

where

$$h_n(\tau,\tau') = 0 \qquad \text{for} \qquad \tau,\tau' < 0 \tag{65}$$

are the Volterra kernels and (64) is the Volterra (functional) series expansion. The forms of the Volterra kernels are impulsive in nature, being the nth order impulse response functions. Equation (64) represents a second-order approximation to the nonlinear process.

The associated Fourier transforms are defined by

$$H_1(\omega) = \int_{-\infty}^{\infty} h_1(\tau)e^{-i\omega\tau}d\tau, \tag{66}$$

$$H_2(\omega,\omega') = \int_{-\infty}^{\infty}\int_{-\infty}^{\infty} h_2(\tau,\tau')e^{-i(\omega\tau+\omega'\tau')}d\tau d\tau', \tag{67}$$

where $H_1(\omega)$ is the Linear Transfer Function (LTF) at the input frequency ω, and $H_2(\omega,\omega')$ is the Quadratic Transfer Function (QTF) corresponding

to a bichromatic input at frequencies ω and ω'. In the case where $y(t)$ is the force on an offshore structure, the QTF is the (complex) amplitude of the second order force acting at the sum frequency $\omega+\omega'$ due to the simultaneous incidence of two waves of frequencies ω and ω'. We consider the case of long crested seas. It may then be shown (Schetzen 1980) that if the input $x(t)$ is a Gaussian process, the two-sided spectrum of the response, $S_{yy}(\omega)$, may be written in terms of the input spectrum, $S_{xx}(\omega)$, as

$$S_{yy}(\omega) = |H_1(\omega)|^2 S_{xx}(\omega) + \int_{-\infty}^{\infty} |H_2(\omega', \omega-\omega')|^2 S_{xx}(\omega') S_{xx}(\omega-\omega') d\omega'. \tag{68}$$

The application of this to springing is discussed by Eatock Taylor (1991).

3.2 *Square law devices*

In order to illustrate the form of second order spectra, and to provide a simple case for testing spectral estimation procedures, we now focus attention on the perfect squarer. Thus in this artificial case the linear transfer function is ignored, and the input-output process is defined by

$$y(t) = x^2(t). \tag{69}$$

We see that in this case the quadratic impulse response function is

$$h_2(\tau, \tau') = \delta(\tau)\delta(\tau'), \tag{70}$$

and the corresponding QTF is

$$H_2(\omega, \omega') = 1. \tag{71}$$

It is clear from Eq. (68) that the spectrum of the squared Gaussian process, here called $S^{*^2}(\omega)$, can be found from the convolution of the spectrum of the input with itself:

$$S^{*^2}(\omega) = \int_{-\infty}^{\infty} S(\omega') S(\omega-\omega') d\omega' \tag{72}$$

The squared signal $x^2(t)$ has a mean component, $\bar{y}$, which can be dealt with in the usual way. The auto-covariance, $C_{yy}(\tau)$, of a random variable y is

$$C_{yy}(\tau) = \langle (y(t)-\overline{y})(y(t+\tau)-\overline{y}) \rangle. \tag{73}$$

Furthermore,

$$\begin{aligned} C_{yy}(\tau) &= \langle y(t)y(t+\tau) - y(t)\overline{y} - y(t+\tau)\overline{y} + \overline{y}^2 \rangle \\ &= \langle y(t)y(t+\tau) \rangle - \overline{y}\langle y(t) \rangle - \overline{y}\langle y(t+\tau) \rangle + \langle y(t) \rangle^2 \\ &= R_{yy}(\tau) - \langle y(t) \rangle^2. \end{aligned} \tag{74}$$

Hence the spectrum of the signal is

$$S_{yy}(\omega) = \frac{1}{2\pi}\int_{-\infty}^{\infty} C_{yy}(\tau)e^{-i\omega\tau}d\tau + \frac{1}{2\pi}\int_{-\infty}^{\infty} \overline{y}^2 e^{-i\omega\tau}d\tau$$

or

$$S_{yy}(\omega) = \frac{1}{2\pi}\int_{-\infty}^{\infty} C_{yy}(\tau)e^{-i\omega\tau}d\tau + \overline{y}^2\delta(\omega). \tag{75}$$

Thus the mean value of the non zero-mean process can be subtracted from the sample without detriment.

3.3 *Analytical spectra*

We next consider a square law device operating on various input spectra. In the context of waves, it is common to define the input by means of a one-sided spectrum. We therefore first convolve a one-sided spectrum with itself, and then consider the implications for a double-sided spectrum. Further details are given in Kernot (1995). We consider the integral

$$G^{*^2}(\omega) = \int_{-\infty}^{0} G(\omega')G(\omega-\omega')\,d\omega' \tag{76}$$

where $G(\omega)$ is a single-sided spectral density. We examine three cases, the first being an input having a rectangular spectrum defined by

$$G(\omega') = \begin{cases} 0 & \omega' < \omega_0 \\ G_0 & \omega_0 \le \omega' \le \omega_1 \qquad (I) \\ 0 & \omega' > \omega_1. \end{cases} \tag{77}$$

Similarly

$$G(\omega-\omega') = \begin{cases} 0 & \omega-\omega' < \omega_0 \\ G_0 & \omega_0 \le \omega-\omega' \le \omega_1 \qquad (II) \\ 0 & \omega-\omega' > \omega_1. \end{cases} \tag{78}$$

The bandwidth is $\Delta = \omega_1 - \omega_0$. The integrand will only be nonzero when conditions (I) and (II) are satisfied, which leads to $2\omega_0 < \omega < 2\omega_1$. It is easy to show that

$$G^{*^2}(\omega) = G_0^2\,(\omega - 2\omega_0) \qquad \text{where} \quad 2\omega_0 \le \omega \le \omega_0 + \omega_1, \tag{79}$$

$$G^{*^2}(\omega) = G_0^2\,(2\omega_1 - \omega) \qquad \text{where} \quad \omega_0 + \omega_1 \le \omega \le 2\omega_1. \tag{80}$$

This convolution of the single sided spectrum with itself, leading to a function which is nonzero over the frequency band $2\omega_0 < \omega < 2\omega_1$, can be

thought of as the sum frequency portion of the output spectrum. This is the primary concern here, but for completeness we can also cover the physically important low, or difference frequency region of the output spectrum, by posing the problem in terms of the equivalent two-sided input spectrum having the same variance. The convolution of the two-sided spectrum with itself results in the two-sided form of the output spectrum, $S^{*^2}(\omega)$, which is symmetrical about $\omega = 0$ with a central peak between $\omega = -\Delta$ and $\omega = \Delta$ of the same shape, but twice the height as that occurring where $2\omega_0 < \omega < 2\omega_1$. The two-sided spectrum $S^{*^2}(\omega)$ has a variance equal to that of $G^{*^2}(\omega)$, namely

$$\sigma^2 = G_0^2 \Delta^2. \tag{81}$$

Next we consider the convolution of a single sided triangular spectrum, specified by the following

$$G(\omega') = \begin{cases} 0 & \omega' < \omega_0 \\ \frac{G_0}{\Delta}(\omega' - \omega_0) & \omega_0 \le \omega' \le \omega_1 \qquad (I) \\ \frac{G_0}{\Delta}(\omega_2 - \omega') & \omega_1 \le \omega' \le \omega_2 \qquad (II) \\ 0 & \omega' > \omega_2 \end{cases} \tag{82}$$

$$G(\omega - \omega') = \begin{cases} 0 & \omega - \omega' < \omega_0 \\ \frac{G_0}{\Delta}(\omega_2 + \omega' - \omega) & \omega_0 \le \omega - \omega' \le \omega_1 \qquad (III) \\ \frac{G_0}{\Delta}(\omega - \omega' - \omega_0) & \omega_1 \le \omega - \omega' \le \omega_2 \qquad (IV) \\ 0 & \omega - \omega' > \omega_2. \end{cases} \tag{83}$$

$\Delta = \omega_1 - \omega_0 = \omega_2 - \omega_1$ is the half bandwidth. The integral in equation (76) can be evaluated for conditions (I, II) with (III, IV) from which it is found that

$$G^{*^2}(\omega) = \left(\frac{G_0}{\Delta}\right)^2 \left\{ \frac{\omega^3}{6} - \omega_0 \omega^2 + 2\omega_0^2 \omega - \frac{4}{3}\omega_0^3 \right\}, \tag{84}$$

where $2\omega_0 \le \omega \le \omega_0 + \omega_1$; and

$$\begin{aligned} G^{*^2}(\omega) &= \left(\frac{G_0}{\Delta}\right)^2 \{ -\frac{\omega^3}{2} + (\omega_0 + 2\omega_1)\omega^2 \\ &+ \left(\omega_0\omega_1 - 3\omega_0\omega_2 - 3\omega_0^2 - \omega_1\omega_2\right)\omega + \frac{1}{3}(\omega_0^3 - \omega_1^3) \\ &+ \omega_0^2(\omega_1 + \omega_2) + \frac{1}{2}\omega_1^2(\omega_0 + \omega_2) - \omega_0\omega_1\omega_2 \} \end{aligned} \tag{85}$$

where $\omega_0 + \omega_1 \le \omega \le 2\omega_1$. The curve $G^{*^2}(\omega)$ is symmetric about $\omega = 2\omega_1$. The variance σ^2 is given by

$$\begin{aligned} \sigma^2 = \quad & \left(\tfrac{G_0}{\Delta}\right)^2 \left(2\omega_0^4 + \omega_0^3\omega_1 + \omega_0^3\omega_2 - 14\omega_0^2\omega_1^2 + 7\omega_0^2\omega_1\omega_2 \right. \\ & \left. + 6\omega_0\omega_1^3 - 6\omega_0\omega_1^2\omega_2 - 2\omega_1^3\omega_2 + 5\omega_1^4\right). \end{aligned} \tag{86}$$

The third case considered here is an input defined by the ISSC wave spectrum (Price & Bishop, 1974)

$$G_{xx}(\omega) = \frac{173 H_s^2}{T_z^4 \omega^5} \exp\left(\frac{-691}{T_z^4 \omega^4}\right) \tag{87}$$

where H_s is the significant wave height and T_z the mean zero crossing period. (The parameters used for the results below were $H_s = 10.0$m and $T_z = 10.0$ sec.) It is not convenient to obtain the convolution in analytical form, but it is simple to evaluate it numerically.

3.4 *Spectra of discrete simulations*

The analytical spectra obtained above are now used to illustrate the reliability of spectral estimates from discrete time series of second order processes. First we review the simulation of the Gaussian process $x(t)$ where the spectrum $G_{xx}(\omega)$ is prescribed. We then consider discrete estimates of the spectra of the simulated processes $x(t)$ and $x^2(t)$.

The random process $x(t)$ can be represented as follows

$$x(t) = \int_0^\infty \sqrt{2G_{xx}(\omega)}\; e^{i\omega t} B(d\omega) \tag{88}$$

where $G_{xx}(\omega)$ represents the one-sided power spectrum of $x(t)$, and the real part of the right hand side here and below is implied. The variable $B(\cdot)$ is defined as a random orthogonal (complex) Gaussian measure.

Equation (88) can now be expressed in discretised form as follows:

$$x(t) \;=\; \sum_{i=1}^{N} [\, 2G_{xx}(\omega_i)\Delta\omega \,]^{\frac{1}{2}} \;\; B_i \, e^{i\omega_i t} \tag{89}$$

where $0 \leq \omega_1 < \omega_2 < \ldots \leq \omega_N$ and are equidistant discretisations of the positive frequency axis. Also

$$\Delta\omega \;=\; \omega_{i+1} - \omega_i$$

and $\{B_i\}$ is a set of independent complex Gaussian numbers with independently distributed real and imaginary parts, having mean zero and unit variance.

The generation of the time history can then utilise the highly efficient inverse FFT algorithm to perform the required summation. An alternative method of simulation has been quite widely used, in which the amplitudes are chosen deterministically, but the phases are random; in effect, B_i in

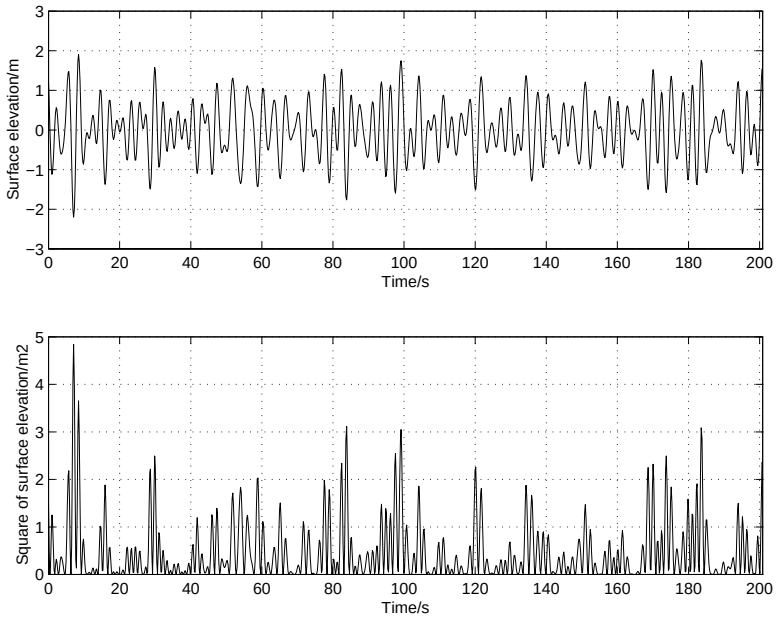

Figure 1: Time history where $x(t)$ has a rectangular spectrum. a) $x(t)$; b) $x^2(t)$.

Eq. (89) is given unit modulus but uniformly distributed random phase. As noted by Tucker *et al.* (1984), however, the spectrum estimated from an input simulated in this manner has no random variability; furthermore, the higher order statistical moments of processes in which the input is so simulated are incorrectly predicted (Langley 1986). It is appropriate therefore to base the following simulations on Eq. (89) with $\{B_i\}$ taken as Gaussian variables with independent real and imaginary parts. As described by Kernot (1995), we create time series $x(t)$ corresponding to the prescribed rectangular, triangular and ISSC spectra described above. The spectra estimated from simulations of $x(t)$, and from the squared process $x^2(t)$, are compared with the analytical spectra.

3.4.1 *Rectangular spectrum*

The discrete form of the problem studied here used an $N = 2048$ point signal and a Nyquist frequency $\omega_{ny} = 16$rad sec^{-1} (see, for example, Newland 1993). The spectrum was defined by Eq. (77), with $\omega_0 = 0.5$ rad sec^{-1}, $\omega_1 = 1.5$ rad sec^{-1} and $G_0 = 1$ m^2 rad^{-1} sec. The corresponding variance is $\sigma^2 = 1$m^2. Figure 1 shows a sample of the time history and its square. Figure 2 shows the effect of frequency smoothing of the raw spectrum. The

process of frequency smoothing can be thought of in terms of positioning a template at the spectral ordinate to be smoothed and finding the sum of all the points covered by the template. The smoothing template is defined as extending $\pm j$ ordinates either side of the central ordinate, the total width being termed aa where $aa = 2j + 1$. A smoothed spectral estimate, $\hat{G}_{xx}(\omega_k)$, is found from

$$\hat{G}_{xx}(\omega_k) = \frac{1}{2j+1} \sum_{l=-j}^{j} G_{xx}(\omega_{k+l}). \tag{90}$$

When smoothing adjacent spectral estimates care must be taken to ensure that the width of the smoothing template is not made too large relative to the rate of change of the spectrum with respect to ω. If the template is too large the smoothing process can result in the artificial redistribution of spectral energy by flattening local extrema. A second problem to arise when smoothing a raw spectral estimate occurs when dealing with a discontinuous function. If the template is placed at (or near) a point of spectral discontinuity, the smoothing process can result in the smearing of spectral energy to regions of the spectrum where, in view of the prescribed spectrum, there should not be any. This can be circumvented by using an adaptive template with narrower widths from $2j$ down to $j+1$ at frequency abscissae adjacent to or at the discontinuity. In the subplots of figure 2 the frequency smoothing is performed with template widths of 1, 3, 5 and 11 points respectively; $aa = 1$ corresponds to the raw spectral estimate. In this and subsequent figures the analytical spectra are also shown for comparison.

The effect of ensemble averaging spectrum of the squared process is presented in figure 3. These are based on averaging over 80 ensembles, and the subplots indicate the further effect of frequency smoothing: $aa = 1$ corresponds to 80 ensembles with no frequency smoothing, and the other subplots show the effect of template widths of 3, 5 and 11 points. Very close agreement is achieved between the analytically and numerically generated curves in this latter case.

3.4.2 *Triangular spectrum*

A discrete signal length of $N = 1024\ (= 2^{10})$ points was used here along with a Nyquist frequency of $\omega_{ny} = 32$ rad sec^{-1}. The spectrum was defined by Eq. (82), with $\omega_0 = 1, \omega_1 = 2, \omega_3 = 3$ rad sec^{-1}, and $G_0 = 1$ m^2 rad^{-1} sec. The corresponding variance is $\sigma = 1$m. Figure 4 shows the raw spectral estimate of the squared time history ($aa = 1$). Ensemble averaged estimates of the spectrum with 160 ensembles are shown in figure 5, together with

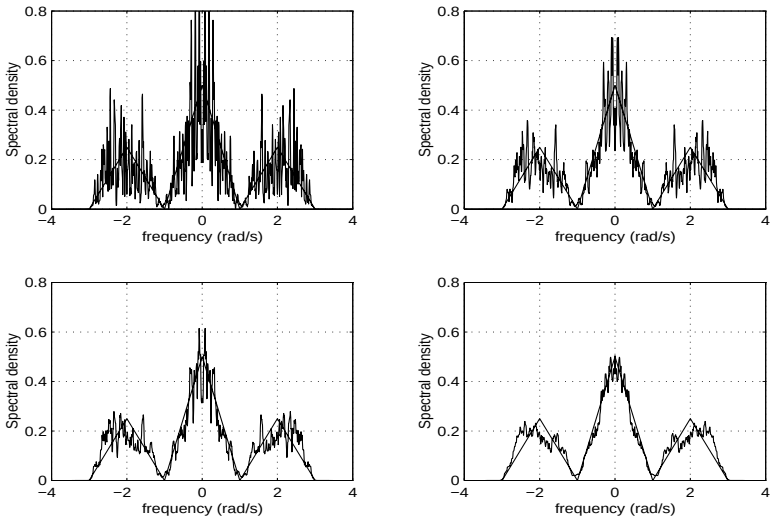

Figure 2: Frequency smoothed spectra of the squared process

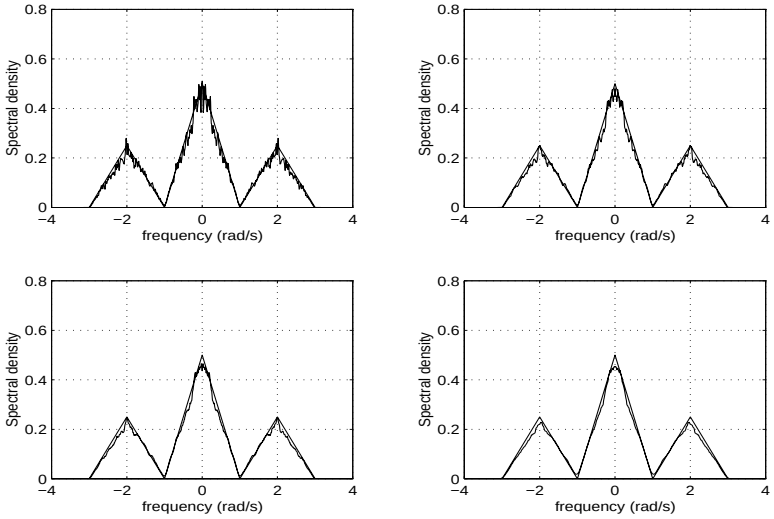

Figure 3: Frequency smoothed and ensemble averaged spectra of the squared process

frequency smoothed estimates using aa=3, 5 and 11 points. The estimated spectra from the discrete simulations of the squared process are again seen to agree very closely with the analytical results.

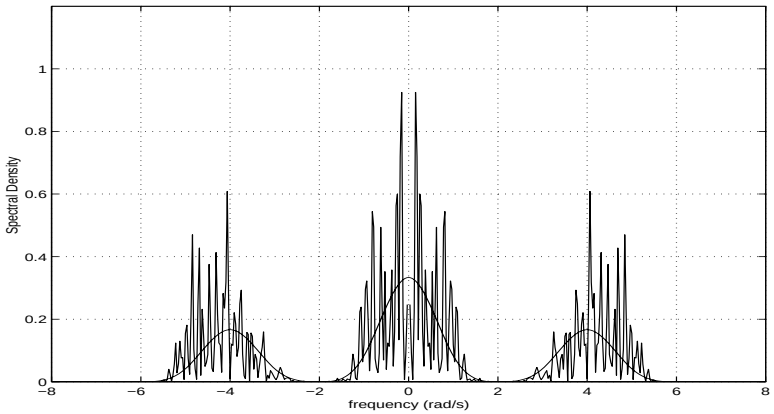

Figure 4: Frequency smoothed spectra of the squared process

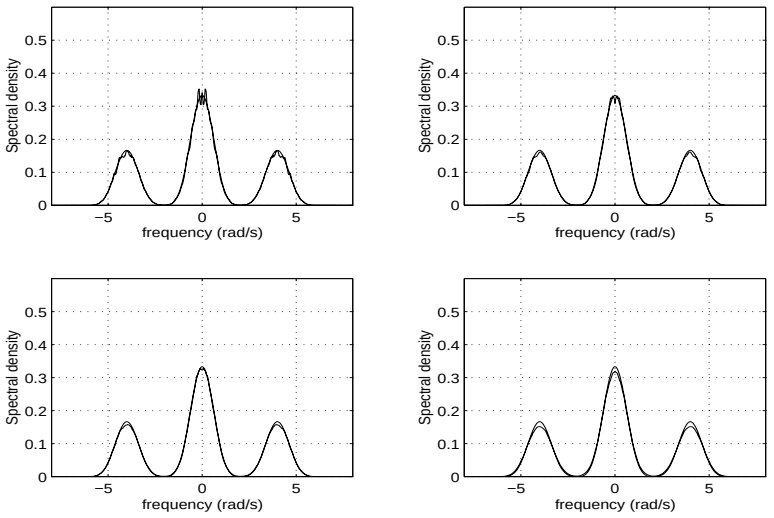

Figure 5: Frequency smoothed and ensemble averaged spectra of the squared process

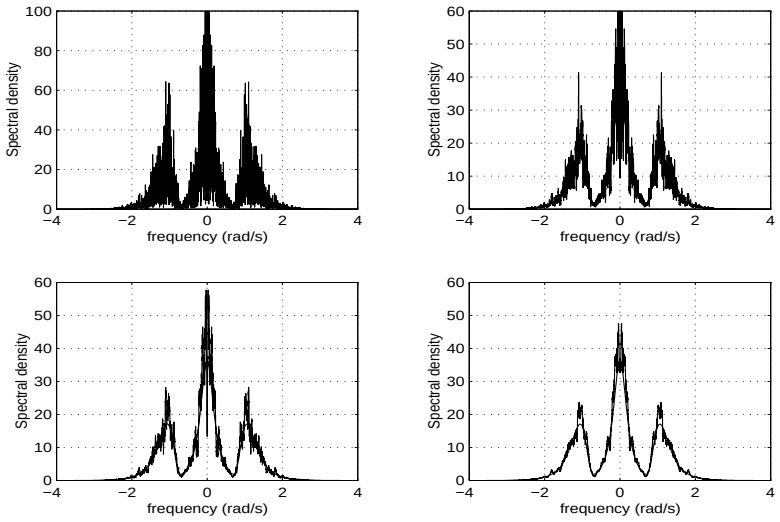

Figure 6: Frequency smoothed spectra of the squared process

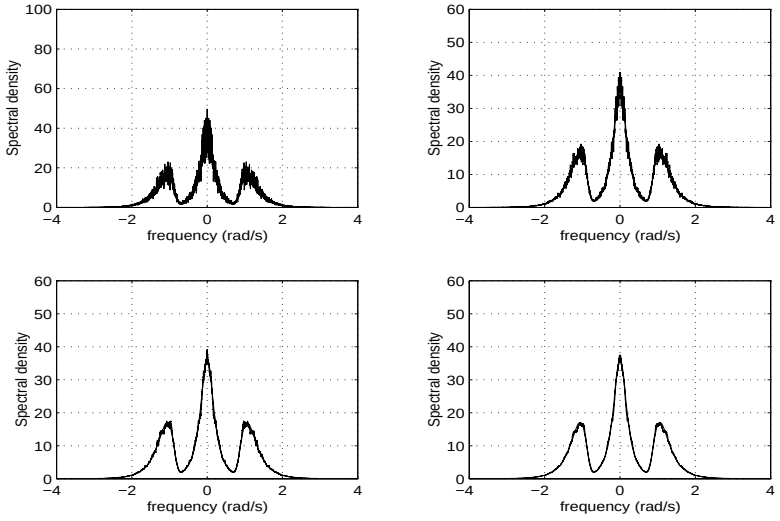

Figure 7: Frequency smoothed and ensemble averaged spectra of the squared process

3.4.3 *ISSC spectrum*

For this example, based on the spectrum defined in (87) and the parameters stated thereafter, a series length of $N = 8192$ $(= 2^{13})$ was used and the Nyquist frequency taken as $\omega_{ny} = 8$ rad sec^{-1}. Figure 6 illustrates the effect of frequency smoothing with aa =1, 5, 13 and 29 points in the smoothing template. Figure 7 shows the effect of this smoothing when used in conjunction with averaging over 160 ensembles. As the frequency resolution was much finer than used in the previous examples, a much wider smoothing template could be employed without causing undue smearing of the peaks.

The FFT-based squared spectral estimation procedure is seen to be able to represent the spectrum of a square law device very accurately once appropriate smoothing techniques have been employed.

4 Probabilistic Descriptions of Second Order Forces and Responses

4.1 *Introduction*

The early development of the theory for describing the response of a general second order system to a Gaussian input is remarkably disjointed, in that gaps of many years pass between successive advances. The breakthrough upon which almost all subsequent works are based was made in 1947 by Kac and Siegert (1947a, b). They obtained an analytical means for determining the characteristic function of a random variable represented by a sum of Gaussian and squared Gaussian random variables, by finding the eigensolution to an integral equation. (The characteristic function is the inverse Fourier transform of the probability density function (PDF) of the random variable.) This classical work, developed for application to fluctuating voltages in radio receivers, was first applied to nonlinear problems in ocean engineering by Neal (1974). He assumed the nonlinear response of a system could be described by a two term Volterra expansion, and applied the Kac-Siegert analysis to determine a closed form for the characteristic function of the response. Neal examined the second order slow drift horizontal motion of a body in waves. A difficulty remained, though, in inverting the characteristic function to obtain the PDF. Surprisingly, almost ten years elapsed before Neal's advances were further developed. Vinje (1983) determined an asymptotic form of the PDF of response of a second order process and also presented a general formulation for the PDF though did not implement it.

Naess (1985) presented a theory for estimating the extreme value and up-crossing frequency of low frequency drift response based on an asymptotic expansion. He notes that the method is applicable when the quadratic (second order) response exceeds the linear response, which is often the case for low frequency responses to second order wave drift forces. The response of a moored system to the second order excitation was modelled as the output from a linear dynamic single degree of freedom system. This effectively assumes that the mooring of the structure behaves linearly. Langley (1987) notes that this is a reasonable assumption given that slow drift motions are lightly damped and the responses near Gaussian.

This analysis was then extended by Naess (1986) who derived a closed form of the PDF for the slow drift response in long crested seas, under the assumption that the forcing was purely quadratic and the high frequency components could be ignored. A simplified model for the combined first and second order extreme slow drift response of a linearly moored floating structure based on the drift period, variance and relative damping was subsequently obtained by Naess (1989). In doing so he also investigated different methods of combining the first and second order responses.

Kato *et al* (1990) developed an approximate method for estimating the statistics of a total low frequency second order response, including a linear component. They showed that the response can be represented by a Laguerre expansion, the first term of which has the form of an exponential (Gamma) PDF. Kato *et al* found that the effect of coupling between the first order and slow drift motions on the PDF varied with the level of damping in the linear dynamic response model.

The Kac-Siegert analysis was extended to multidirectional, short crested seas by Naess (1990) leading to a rather complex formulation for the prediction of slow drift motions. This of course encountered the significant difficulty of estimating the bidirectional quadratic transfer function, which Naess circumvented by various approximations. The theory was extended to investigate the sum frequency springing responses by Naess & Ness (1992). A sum frequency approximation was employed to exclude the low frequency response components, and the PDF was evaluated by a numerical integration procedure. They found that the forcing and response statistics were approximately exponentially distributed leading to much greater estimated probabilities at extremes than would be predicted by a Gaussian distribution. Langley & McWilliam (1993) tackled the problem of determining the joint PDF of the first order and slow drift motions based on the Kac-Siegert analysis solution, and obtained a closed form expression for the joint PDF in the form of a series involving the eigenvalues of the matrix approximating the integral equation in the Kac-Siegert formulation. This approach was extended by McWilliam & Langley (1993) to investigate the

extreme statistics of combined first and second order slow drift motions of a body in waves.

Attempts have been made to examine the statistics of nonlinearly moored offshore structures by considering the response to be a Markov random process (the basic theory for which can be found in Lin 1967). Computation of the PDF of a Markov process requires the solution of the Fokker-Planck-Kolmogorov (FPK) equation, an early attempt at which in a marine context was made by Roberts (1981). The excitation was assumed to be Gaussian white noise, which does facilitate a solution but has practical limitations. More recently Naess & Johnsen (1993) applied a numerical path integration scheme to the FPK equation to investigate the slow drift motion of a nonlinearly moored structure. For the purely quadratic excitation which they investigated, they found their numerical approach yielded highly accurate results. McWilliam & Langley (1994) considered the combined response of a system and applied a complex functional expansion technique to the solution of the FPK equation. The nonlinearity in the mooring system was modelled by introducing a cubic stiffness term into the linear dynamic response equation.

Scarcity of sum frequency QTF data has forced the emphasis of previous statistical investigations of second order processes to focus largely on the slow drift behaviour of a compliant offshore structure. As a result of this, the statistics of high frequency vertical resonant responses of a tensioned buoyant platform are comparatively unknown. However, obtaining a probabilistic description of the second order springing response is of importance if accurate assessment of the fatigue life of the tethers is to be made. It can also lead to an estimate of the extreme response behaviour of a compliant structure to second order high frequency loading. Large displacements in the stiff response modes that may occur at resonance of a tautly moored compliant structure may affect the operational performance of the structure. In the rest of this section we review the application of the Kac-Siegert analysis to high frequency springing. We then compare the results with statistics generated from Monte Carlo simulations using the method of generating wave records described in the previous section. This is illustrated in the context of a Tension Leg Well Control Station. The wave excitation was computed from the nonlinear wave diffraction program *DIFFRACT* described in Section 2, leading to LTF and QTF data tailored to a specific springing problem (unlike other published Kac-Siegert analyses, which generally have been concerned with highly idealised problems).

4.2 *Discretised Kac-Siegert analysis*

The Fourier transform of second order output is related to the Fourier transform of the input through the QTF

$$Y(\omega,\omega') = H_2(\omega,\omega')X(\omega)X(\omega'). \tag{91}$$

Analogous to Eq (88) we can write a time domain simulation of second order output as

$$y(t) = \int_{-\infty}^{\infty}\int_{-\infty}^{\infty} H_2(\omega,-\omega')\sqrt{G_{xx}(|\omega|)G_{xx}(|\omega'|)}\, e^{i(\omega-\omega')t} B(d\omega)B(d\omega')^*, \tag{92}$$

noting $B[d(-\omega)] = B[d\omega]^*$. This is based on the sum frequency approximation

$$H_2(\omega,-\omega') = 0 \qquad \text{for } \omega\cdot\omega' > 0,$$

and implies that all difference frequency components of the second order excitation forces are neglected and only sum frequency terms retained. As before, G_{xx} is the one sided input spectrum, and in what follows we designate this G_η, to indicate that wave elevation $\eta(t)$ is the input. We also replace $y(t)$ by $f_2(t)$ to designate the second order force.

Equation (92) can then be expressed in discretised form

$$f_2(t) = \sum_{i=-M}^{M}\sum_{j=-M}^{M} [G_\eta(|\omega_i|)G_\eta(|\omega_j|)]^{\frac{1}{2}}\,\Delta\omega\, H_2(\omega_i,-\omega_j)\, B_iB_j^*\, e^{i(\omega_i-\omega_j)t}, \tag{93}$$

in which the summations over the frequency ordinates i and j omit zero. Also, the complex Gaussian numbers B_i satisfy

$$B_{-i} = B_i^* \qquad i = 1,...,M,$$

and

$$\langle B_iB_j^*\rangle = \delta_{ij}\,,$$

where $i,j = -M,...,-1,\ 1,...,M$. For calculating the response of the structure, $\xi_2(t)$, to the second order excitation, we adopt a linearised equation of motion. We thus write (using the first term in the Volterra series)

$$\xi_2(t) = \int_{-\infty}^{\infty} \hat{h}_1(\tau)f_2(t-\tau)\,d\tau \tag{94}$$

in which $\hat{h}_1(\tau)$ is the linear impulse response function of the dynamic system linking response $\xi(t)$ to force $f(t)$. (The lower limit of integration may be set to zero for a causal system.)

The quadratic impulse response function, $k_2(\tau,\tau')$, linking response to wave input may be defined as

$$k_2(\tau,\tau') = \int_{\infty}^{\infty} \hat{h}_1(s)\, h_2(\tau - s, \tau' - s)\; ds, \tag{95}$$

whence the second order response is

$$\xi_2(t) = \int_{\infty}^{\infty}\int_{\infty}^{\infty} k_2(\tau,\tau')\, \eta(t-\tau)\, \eta(t-\tau') d\tau d\tau'. \tag{96}$$

The QTF corresponding to $k_2(\tau,\tau')$ can be shown to be (*e.g.* Naess & Johnson 1993)

$$K_2(\omega\,,\omega') = \hat{H}_1(\omega+\omega')H_2(\omega,\omega'), \tag{97}$$

where $\hat{H}_1(\omega)$ is the linear transfer function for the dynamic systemm, the Fourier transform of $\hat{h}_1(t)$ in Eq. (94). It follows from Eq. (92) and Eq. (97) that

$$\xi_2(t) = \int_{-\infty}^{\infty}\int_{-\infty}^{\infty} K_2(\omega\,,-\omega')\sqrt{G_\eta(|\omega|)G_\eta(|\omega'|)}\, e^{\,i(\omega-\omega')t} B(d\omega)B(d\omega')^*. \tag{98}$$

Equation (98) can be re-written

$$\xi_2(t) = \int_{-\infty}^{\infty}\int_{-\infty}^{\infty} \Gamma(\omega\,,\omega')\, e^{\,i(\omega-\omega')t} B(d\omega)B(d\omega')^* \tag{99}$$

where the kernel function $\Gamma(\omega,\omega')$ has been introduced such that

$$\Gamma(\omega,\omega') = \sqrt{G_\eta(|\omega|)}\; K_2(\omega,-\omega')\; \sqrt{G_\eta(|\omega'|)}. \tag{100}$$

We now develop the analysis in discretised form. The response to the sum frequency excitation can be expressed as

$$\begin{aligned}\xi_2(t) = \sum_{i=-M}^{M}\sum_{j=-M}^{M} \frac{1}{2}\,[G_\eta(|\omega_i|)G_\eta(|\omega_j|)]^{\frac{1}{2}}\,\Delta\omega \\ \times\; H_1(\omega_i-\omega_j)H_2(\omega_i,-\omega_j)\; B_i B_j^*\, e^{\,i(\omega_i-\omega_j)t}.\end{aligned} \tag{101}$$

Equation (100) can be written

$$\Gamma_{ij} = \frac{1}{2}\,[G_\eta(|\omega_i|)G_\eta(|\omega_j|)]^{\frac{1}{2}}\,\Delta\omega\; K_2(\omega_i,-\omega_j), \tag{102}$$

and substituting this expression into equation (101) leads to

$$\xi_2(t) = \sum_{i=-M}^{M} \sum_{j=-M}^{M} \Gamma_{ij}\ B_i B_j^* e^{i(\omega_i - \omega_j)t}. \tag{103}$$

From this point onwards the focus of the analysis will be directed towards the second order response but the results could easily be applied to second order forces.

As in the difference frequency problem (Langley 1987, Naess 1986), we now seek to express $\xi_2(t)$ as a single summation, by using the eigenvalues and eigenvectors of the appropriate matrix of QTFs. The sum frequency problem is slightly more complex, and we follow the development given by Naess & Ness (1992). Considering the symmetries of the quadratic transfer function $K_2(\omega, -\omega')$ shows that the discretised form of the kernel satisfies

$$\Gamma_{ij} = \Gamma_{ji}^* \tag{104}$$

where $i, j = -M, ..., -1, 1, ..., M$. The discretised form of the sum frequency approximation introduced previously leads to

$$\Gamma_{ij} = 0 \quad \text{for} \quad i \cdot j > 0. \tag{105}$$

We now apply a transformation to the kernel Γ_{ij}, so that the quadratic form in (103) can be expressed by means of a single summation. Hence we examine an eigenvalue problem in the form

$$\sum_{j=-M}^{M} \Gamma_{ij} v(\omega_j) = \lambda v(\omega_i) \tag{106}$$

where the summation excludes the term corresponding to zero frequency. This can be written in matrix form as

$$\boldsymbol{T}\boldsymbol{v} = \lambda \boldsymbol{v} \tag{107}$$

where the matrix $\boldsymbol{T}$, of order $2M \times 2M$, is

$$\boldsymbol{T} = \begin{pmatrix} \boldsymbol{\emptyset} & \boldsymbol{S} \\ \boldsymbol{S}^H & \boldsymbol{\emptyset} \end{pmatrix}. \tag{108}$$

Here $\boldsymbol{\emptyset}$ is a square null matrix of order $M \times M$ and the terms of $\boldsymbol{S}$ are

$$S_{ij} = \Gamma_{-M-1+i,j}. \tag{109}$$

$\boldsymbol{S}^H = (\boldsymbol{S}^*)^T$ is the Hermitian conjugate of $\boldsymbol{S}$. It is assumed that $\boldsymbol{S}$ and therefore $\boldsymbol{T}$ are non-singular matrices. In equation (107), λ_α and $\boldsymbol{v}_\alpha$ denote the eigenvalues and orthonormal eigenvectors of $\boldsymbol{T}$, that is

$$\boldsymbol{v}_\alpha = (v_{\alpha,-M}, ..., v_{\alpha,-1}, v_{\alpha,1}, ..., v_{\alpha,M})^T \quad \text{and} \quad \alpha = (-M, ..., -1, 1, ..., M).$$

The elements of the eigenvectors are written as $v_\alpha(\omega_i)$.

In order to find the eigenvalues of the matrix $\boldsymbol{T}$ Naess and Ness (1992) note that the matrix $\boldsymbol{S}^H\boldsymbol{S}$ is a Hermitian non-negative matrix, which implies that all the eigenvalues are non-negative. Also, it can be shown that if μ is an eigenvalue of $\boldsymbol{S}^H\boldsymbol{S}$, then $\pm\sqrt{\mu}$ must be eigenvalues of $\boldsymbol{T}$. This in turn implies that if λ is an eigenvalue of $\boldsymbol{T}$ then so is $-\lambda$ and further, that λ is real. Therefore if μ_α, $\alpha = 1, ..., M$, are the eigenvalues of $\boldsymbol{S}^H\boldsymbol{S}$, then λ_α, $\alpha = -M, ..., -1, 1, ...M$, defined by

$$\lambda_\alpha = -\sqrt{\mu_{|\alpha|}} \quad \alpha = -M, ..., -1 \tag{110}$$

$$\lambda_\alpha = \sqrt{\mu_\alpha} \quad \alpha = 1, ..., M \tag{111}$$

are the eigenvalues of $\boldsymbol{T}$. The eigenvector $v(\omega_i)$ corresponds to the eigenvalue λ in equation (106). A vector quantity $\hat{v}(\omega_i)$ is now defined as the eigenvector corresponding to the eigenvalue $-\lambda$,

$$\hat{v}(\omega_i) = \chi(\omega_i)v(\omega_i), \tag{112}$$

and Naess and Ness (1992) show that

$$\begin{aligned} \chi(\omega_i) &= \sqrt{-1} \quad \text{for} \quad \omega_i < 0 \\ \chi(\omega_i) &= -\sqrt{-1} \quad \text{for} \quad \omega_i > 0. \end{aligned} \tag{113}$$

The eigen decomposition then leads to

$$\Gamma_{ij} = \sum_{\alpha=1}^{M} \lambda_\alpha \left\{ v_\alpha(\omega_i)\, v_\alpha(\omega_j)^* - v_{-\alpha}(\omega_i)\, v_{-\alpha}(\omega_j)^* \right\} \tag{114}$$

where $v_{-\alpha}(\cdot) = \hat{v}_\alpha(\cdot)$. This may now be substituted into equation (103) for the second order response to give

$$\xi_2(t) = \sum_{\alpha=1}^{M} \lambda_\alpha \left(W_\alpha(t)^2 - W_{-\alpha}(t)^2 \right) \tag{115}$$

where

$$W_\beta(t) = \sum_{i=-M}^{M} v_\beta(\omega_i)\, B_i\, e^{i\omega_i t}. \tag{116}$$

$W_\beta(t)$ are zero mean Gaussian processes, $(\beta = -M, ..., -1, 1, ...M)$, that are both real and stationary. Equation (115) is equivalent to equation (103), following the eigen transformation.

The nth order cumulant of the process, k_n, is given by Kato *et al* (1990), as

$$k_n = \sum_\alpha 2^{n-1}(n-1)!\,\lambda_\alpha^n. \tag{117}$$

In particular, the first four cumulants, k_n, $n = 1, ..., 4$ of the process can be determined from equation (117) as:

$$\langle \xi_2(t) \rangle = k_1 = \sum_{\alpha=-M}^{M} \lambda_\alpha = 0, \tag{118}$$

$$\langle \xi_2^2(t) \rangle = k_2 = 4 \sum_{\alpha=1}^{M} \lambda_\alpha^2, \tag{119}$$

$$k_3 = 8 \sum_{\alpha=-M}^{M} \lambda_\alpha^3 = 0, \tag{120}$$

$$k_4 = 96 \sum_{\alpha=1}^{M} \lambda_\alpha^4. \tag{121}$$

The kurtosis, γ, is defined as

$$\gamma = \frac{k_4}{k_2^2}, \tag{122}$$

and for a Gaussian distributed variable, $\gamma = 3$.

In general the response $\xi(t)$ contains both first and second order components. It is possible and convenient to express the first order component also in terms of the eigenprocesses, $W_\beta(t)$. Thus $\xi_1(t)$ is first written in a form analogous to equation (101), as

$$\xi_1(t) = \sum_{i=-M}^{M} H_1(\omega_i) \sqrt{\frac{1}{2} G_\eta(|\omega_i|) \Delta\omega}\, B_i e^{i\omega_i t}. \tag{123}$$

Here $H_1(\omega)$ is the linear transfer function between wave elevation $\eta(t)$ and response $\xi(t)$.

We next use the orthonormal vectors v_α to write

$$H_1(\omega_i) \sqrt{\frac{1}{2} G_\eta(|\omega_i|) \Delta\omega} = \sum_{\alpha=-M}^{M} c_\alpha v_\alpha(\omega_i), \tag{124}$$

where the coefficients c_α are obtained by taking advantage of the orthonormality of the eigenvectors. Thus

$$c_\alpha = \sum_{i=-M}^{M} H_1(\omega_i)\sqrt{\frac{1}{2}G_\eta(|\omega_i|)\Delta\omega}\; v_\alpha(\omega_i). \tag{125}$$

If equation (125) is substituted into equation (123) and the definition of W_β recalled from equation (116), the following representation is found:

$$\xi_1(t) = \sum_{\alpha=-M}^{M} c_\alpha W_\alpha(t). \tag{126}$$

The random variable $\xi(t)$ representing the combined first and second order response is thus

$$\xi = \sum_{\alpha=1}^{M}\{\lambda_\alpha(W_\alpha^2 - W_{-\alpha}^2) + c_\alpha W_\alpha - c_{-\alpha}W_{-\alpha}\}. \tag{127}$$

The random process ξ can be described by its characteristic function, $M_\xi(\theta)$ (see for example Papoulis 1991):

$$M_\xi(\theta) = \langle e^{i\theta\xi}\rangle = \int_{-\infty}^{\infty} p_\xi(x)\quad e^{i\theta x}\;\; dx. \tag{128}$$

where $_\xi(x)$ is the probability density function. Consider first just one of the α processes. A random process U can then be written

$$U = \lambda W^2 + cW \tag{129}$$

which has the characteristic function, $M_U(\theta)$, defined as

$$\begin{aligned} M_U(\theta) &= \int_{-\infty}^{\infty} p_U(u)\; e^{i\theta u}\; du \\ &= \langle e^{i\theta u}\rangle = \int_{-\infty}^{\infty} e^{i\theta(\lambda w^2 + cw)}\; p_W(w)\; dw, \end{aligned} \tag{130}$$

in which u and w are the state variables corresponding to the random processes U and W respectively. If the probability density function of the unit Gaussian process W,

$$p_W(w) = \frac{1}{\sqrt{2\pi}}.e^{-\frac{w^2}{2}},$$

is substituted into equation (130), we obtain

$$M_U(\theta) = \frac{1}{\sqrt{2\pi}} \int_{-\infty}^{\infty} \exp[-w^2(\frac{1}{2} - i\lambda\theta) + ic\theta w] \; dw. \tag{131}$$

The integral in equation (131) is rewritten in line with the approach described by Kac and Siegert (1947),

$$\begin{aligned} M_U(\theta) &= \frac{1}{\sqrt{2\pi}} \int_{-\infty}^{\infty} \exp\{-\left(w\sqrt{\frac{1}{2} - i\lambda\theta} - \frac{ic\theta}{2\sqrt{\frac{1}{2} - i\lambda\theta}}\right)^2 \\ &- \frac{c^2\theta^2}{4(\frac{1}{2} - i\lambda\theta)}\} \; dw \\ &= \frac{1}{\sqrt{2\pi}} \exp\left(\frac{-c^2\theta^2}{4(\frac{1}{2} - i\lambda\theta)}\right) \\ &\times \int_{-\infty}^{\infty} \exp\left\{-\left(w\sqrt{\frac{1}{2} - i\lambda\theta} - \frac{ic\theta}{2\sqrt{\frac{1}{2} - i\lambda\theta}}\right)^2\right\} \; dw \end{aligned} \tag{132}$$

With the change of variable

$$\gamma = w\sqrt{\frac{1}{2} - i\lambda\theta} - \frac{ic\theta}{2\sqrt{\frac{1}{2} - i\lambda\theta}}, \tag{133}$$

Eq. (132) becomes

$$M_U(\theta) = \frac{1}{\sqrt{\pi(1 - i2\lambda\theta)}} \exp\left(\frac{-c^2\theta^2}{2(1 - i2\lambda\theta)}\right) \int_{-\infty}^{\infty} \exp(-\gamma^2) \; d\gamma. \tag{134}$$

The integral in Eq. (134) has the form of the error function and over the infinite limits has the value $\sqrt{\pi}$. Thus the characteristic function $M_U(\theta)$ reduces to

$$M_U(\theta) = \frac{1}{\sqrt{1 - i2\lambda\theta}} \cdot \exp\left(\frac{-c^2\theta^2}{2(1 - i2\lambda\theta)}\right). \tag{135}$$

A similar analysis for a random process V, defined by $V = -\lambda W^2 + \hat{c}W$, leads to the characteristic function

$$M_V(\theta) = \frac{1}{\sqrt{1 + i2\lambda\theta}} \exp\left(\frac{-\hat{c}^2\theta^2}{2(1 + i2\lambda\theta)}\right). \tag{136}$$

The characteristic function of a random process which is itself the sum of two independent random processes is found by taking the product of the

characteristic functions of the two processes. The characteristic function of a process resulting from the sum of U and V is hence found from

$$\begin{aligned} M_{U+V}(\theta) &= M_U(\theta) \cdot M_V(\theta) \\ &= \frac{1}{\sqrt{1+4\lambda^2\theta^2}} \exp\left(-\frac{c^2\theta^2}{2(1-i2\lambda\theta)} - \frac{\hat{c}^2\theta^2}{2(1+i2\lambda\theta)}\right) \end{aligned} \quad (137)$$

Recalling now the definition of the random process ξ in equation (127), which is the sum of such processes U_α and V_α, we see that the characteristic function $M_\xi(\theta)$ can be obtained from the product of the individual functions $M_{U+V}(\theta)$:

$$M_\xi(\theta) = \prod_\alpha \left[\frac{1}{\sqrt{1+4\lambda_\alpha^2\theta^2}} \exp\left\{-\frac{c_\alpha^2\theta^2}{2(1-i2\lambda_\alpha\theta)} - \frac{c_{-\alpha}^2\theta^2}{2(1+i2\lambda_\alpha\theta)}\right\}\right]. \quad (138)$$

The probability density function, $p_\Xi(\xi)$ of the random process ξ is then given by the inverse Fourier transform of the characteristic function $M_\xi(\theta)$:

$$p_\Xi(\xi) = \frac{1}{2\pi}\int_{-\infty}^{\infty} M_\xi(\theta)\ \exp(-i\theta\xi)\ \ d\theta. \quad (139)$$

Upon substitution of the characteristic function $M_\xi(\theta)$ from Eq. (138) into Eq. (139), this becomes

$$\begin{aligned} p_\Xi(\xi) &= \frac{1}{2\pi}\int_{-\infty}^{\infty} \exp(-i\theta\xi) \prod_\alpha \frac{1}{\sqrt{1+4\lambda_\alpha^2\theta^2}} \\ &\times \exp\left\{-\frac{c_\alpha^2\theta^2}{2(1-i2\lambda_\alpha\theta)} - \frac{c_{-\alpha}^2\theta^2}{2(1+i2\lambda_\alpha\theta)}\right\}\ d\theta. \end{aligned} \quad (140)$$

It is noted here that

$$(1+4\lambda^2\theta^2)^{-\frac{1}{2}} = \exp\left[\ln\{(1+4\lambda^2\theta^2)^{-\frac{1}{2}}\}\right] = \exp\left[-\frac{1}{2}\ln(1+4\lambda^2\theta^2)\right], \quad (141)$$

and if the substitution $s = i\theta$ is made, the characteristic function can be rewritten as follows:

$$M_\xi(s) = \prod_\alpha \left[\exp\left\{-\frac{1}{2}\ln(1-4\lambda_\alpha^2 s^2) + \frac{c_\alpha^2 s^2}{2(1-2\lambda_\alpha s)} + \frac{c_{-\alpha}^2 s^2}{2(1+2\lambda_\alpha s)}\right\}\right]. \quad (142)$$

The PDF can then be written

$$\begin{aligned} p_\Xi(\xi) = \frac{1}{i2\pi}\int_{-i\infty}^{i\infty} & \exp(-s\xi) \prod_\alpha \exp\left\{-\frac{1}{2}\ln(1-4\lambda_\alpha^2 s^2)\right. \\ & \left. + \frac{c_\alpha^2 s^2}{2(1-2\lambda_\alpha s)} + \frac{c_{-\alpha}^2 s^2}{2(1+2\lambda_\alpha s)}\right\}\ ds. \end{aligned} \quad (143)$$

The product in the integrand of Eq. (143) can now be replaced by a summation and leads to

$$p_{\Xi}(\xi) = \frac{1}{i2\pi}\int_{-i\infty}^{i\infty} \exp\left[-s\xi + \sum_{\alpha}\left\{-\frac{1}{2}\ln(1-4\lambda_{\alpha}^2 s^2) + \frac{c_{\alpha}^2 s^2}{2(1-2\lambda_{\alpha}s)} + \frac{c_{-\alpha}^2 s^2}{2(1+2\lambda_{\alpha}s)}\right\}\right] ds. \quad (144)$$

This integral may then be evaluated by the method of steepest descent and numerical integration through the saddle point, as described by Naess & Ness (1992) and Kernot (1995).

This concludes the Kac-Siegert analysis. It shows that computation of the required PDF is based upon determining the eigensolution of the Hermitian matrix, $\boldsymbol{T}$, in Eq. (107). The level of discretisation needed over the bifrequency plane is governed by how rapidly the QTF is varying and also how finely tuned the response of the system is, as defined by the equation for $H_1(\omega_1+\omega_2)$. The finer the resolution the greater the computational task involved in determining the eigensolution of $\boldsymbol{T}$. Langley & McWilliam (1993) note that, in general, of the order of one hundred frequency components are typically required to describe accurately the kernel function Γ_{ij} of Eq. (102).

4.3 *Numerical experiments for a taut moored platform*

The method described above has been implemented for a tension leg well control station (TLWCS), which is a novel form of compliant structure. The TLWCS comprises a water-tight, cylindrical-sectioned hull connected to the sea bed by a single tether. The top and bottom tether connections are made by use of flex-joints which help to alleviate the bending moment generated at the base of the hull as the buoy heels. The tension in the tether is developed by the excess buoyancy resulting from pulling the hull down below its free floating equilibrium position in the same way that TLP tethers are tensioned. The use of a single tether in the TLWCS means that the hull is hydrostatically restrained in pitch/roll but, unlike the TLP, it does not have the restraint associated with differentially loaded separated tethers. Heeling motion then has to be restrained by hydrostatic stiffness and inertia alone. Greater explanation of the operational and design characteristics of the TLWCS are described in Brooking & Jefferys (1990). For the case studied here, the hull below the water line is cylindrical with a diameter of 8.0m to a depth of 20m and then tapers linearly down to the flex-joint at a depth of 27m, where it is attached to the tether. The hull has a mass of 668×10^3kg in air, and the TLWCS is designed to operate in a range of depths from 150m to 450m.

The persistent vertical resonance associated with springing may be of great significance to the TLWCS in terms of the expected tether fatigue. If this second order effect were not accounted for in the design process, a serious underprediction of the wear on the tether could be made. The basic methodology employed here is one of direct simulation of the various quantities involved such as wave elevation, sum frequency heave force and vertical response The hydrodynamic analysis of the TLWCS, including the calculation of first and second order forces, was performed with the boundary element program *DIFFRACT* discussed above. Time histories of first and second order response in simulated random waves were created, from which statistics of the response were obtained using standard techniques. The linear and quadratic transfer functions were also used in a probabilistic Kac-Siegert analysis along the lines presented here, to yield analytical estimates of the corresponding probability densities for the responses. From the statistical analysis, estimates of the cumulants were also obtained, and compared with estimates from the eigenvalues derived from the Kac-Siegert analysis.

Results for the cumulants are shown in table 10. Values are given relating to the second order heave force on the TLWCS, and the total heave responses corresponding to two levels of damping of heave motions: 0.05% and 0.15% of critical damping respectively. (These values are assumed to account for damping of both mechanical and hydrodynamic origin - a discussion of the relative contributions to damping in vertically tethered offshore structures may be found in Kim & Yue, 1988 and Kernot, 1995). These and subsequent results were calculated for a sea state having an ISSC spectrum with $H_s = 5.0$ m and $T_z = 5.0$ sec, which causes significant sum frequency excitation at the heave resonance of this structure. (The heave resonant frequency was 3.47 rad sec^{-1}, corresponding to a period of 1.81 sec.) The quadratic transfer functions were evaluated over the ranges $3.4 \leq \omega_1 + \omega_2 \leq 3.55$ rad sec^{-1} and $0 \leq \omega_1 - \omega_2 \leq 1.5$ rad sec^{-1}. This covered the range over which most of the second order excitation was concentrated. The simulations were based on time series of 32768 points, with a time step $\Delta t = 0.3067$ sec, corresponding to a record length of almost three hours.

Table 10 also lists the largest eigenvalue, λ_{max}, from the Kac-Siegert analysis for the second order process. For the second order force this is found to be approximately 20% of the standard deviation. For the heave response the largest eigenvalue is approximately 7% of the standard deviation for the more lightly damped case and around 9% for the more heavily damped case. The estimates of the kurtosis, γ, in table 10 show that the second order force is distinctly non-Gaussian, with a value substantially greater than the Gaussian result $\gamma = 3$. The lightly damped response has a

Table 10: Cumulant data for second order force and total response

	F_2/N	ξ_2/m (0.05%)	ξ_2/m (0.15%)
k_2 simulated	6.34e06	6.55e-04	5.05e-05
k_2 Kac-Siegert	6.53e06	5.62e-04	5.27e-05
k_4 Kac-Siegert	2.20e14	1.09e-06	9.95e-09
λ_{max}	5.15e02	1.77e-03	6.72e-04
$\gamma = \frac{k_4}{k_2^2}$	5.16	3.44	3.58

Table 11: Eigenvalues and weighting parameters, second order heave force

α	$\lambda_\alpha(N)$	$c_\alpha(N)$	$c_{-\alpha}(N)$
1	5.14772e+02	1.70766e+02	4.43122e+02
2	4.24759e+02	7.99915e+02	3.89146e+02
3	3.47745e+02	1.19174e+03	3.03318e+02
4	2.80187e+02	1.49219e+03	-2.14927e+02
5	2.20172e+02	7.85768e+02	-9.09248e+02
6	1.64182e+02	4.56752e+02	-1.09104e+03
7	1.16699e+02	2.39943e+02	6.65685e+02
8	1.11366e+02	6.78635e+03	5.20325e+02
9	1.08550e+02	5.09278e+01	2.91232e+02
10	1.08363e+02	1.54617e+02	1.76763e+02

kurtosis closer to 3, and there is a slight increase with damping indicating that the distribution is becoming less Gaussian with increasing damping.

Stansberg (1991) has developed a model based on a similar form of eigen transformation, for low frequency second order forces and motions. He investigated a large range of damping values and found that for very heavy damping the set of eigenvalues obtained was dominated by one very large eigenvalue. On the other hand, for lightly damped responses the eigenvalues obtained were approximately equal. A comparison of the weighting factors, c_α, and λ_α, describing the first and second order components of heave force as defined in equation (127) is presented in table 11. The eigenvalues, λ_α, in the table are the largest ten found in the analysis and it is seen that there is no one dominant value, the largest being approximately 20% greater than the second largest. The corresponding weighting factors of the first order process, c_α, are generally of the same order of magnitude as the coefficients, λ_α.

Table 12 presents the coefficients of the first and second order response process where the damping is $c_{33} = 0.05\%$. The eigenvalues, λ_α, for this

Table 12: Eigenvalues and weighting parameters, response with 0.05% damping

α	λ_α (mm)	c_α (mm)	$c_{-\alpha}$ (mm)
1	1.77053e+00	3.46616e-03	1.28927e-02
2	1.73200e+00	-2.60112e-04	5.99300e-04
3	1.73131e+00	5.67473e-04	3.44946e-04
4	1.72135e+00	4.32601e-04	-5.29434e-04
5	1.71081e+00	1.93569e-03	-1.75671e-03
6	1.70397e+00	4.97964e-04	-5.17120e-03
7	1.69493e+00	-9.61285e-04	-1.06426e-03
8	1.67505e+00	2.90932e-03	5.82101e-03
9	1.64851e+00	1.85190e-04	2.58515e-03
10	1.64531e+00	8.07078e-03	-1.64525e-03

Table 13: Eigenvalues and weighting parameters, response with 0.15% damping

α	λ_α (mm)	c_α (mm)	$c_{-\alpha}$ (mm)
1	6.72145e-01	-9.61572e-03	2.09314e-02
2	5.88106e-01	2.35014e-03	-5.18423e-03
3	5.24946e-01	-1.82365e-04	1.72041e-04
4	5.23524e-01	-1.06366e-03	1.99511e-03
5	5.19446e-01	-1.01685e-03	-3.31805e-03
6	5.16369e-01	-2.45679e-04	-2.56316e-03
7	5.07619e-01	-6.78825e-04	-6.25987e-04
8	5.01115e-01	-9.20835e-04	1.39177e-03
9	4.95843e-01	-2.57206e-04	1.75317e-03
10	4.88934e-01	-6.37519e-04	-4.06218e-04

analysis are seen to be approximately equal. This finding agrees with that of Stansberg (1991) when the response of the system is very lightly damped. Also of note are the very small first order response weighting factors which result from the extremely low value of the frequency response function, $\hat{H}_1(\omega)$, at typical wave frequencies well away from the resonant frequency.

The weighting coefficients for the response with a damping level of $c_{33} = 0.15\%$ are presented in table 13. Greater variation is seen in the eigenvalues, λ_α, the largest being approximately 15% greater than the second largest. Once again, the first order coefficients, c_α, are very small relative to the second order weighting coefficients. Similar conclusions may be drawn from results obtained for greater damping.

The PDFs for heave force and response computed by direct numerical

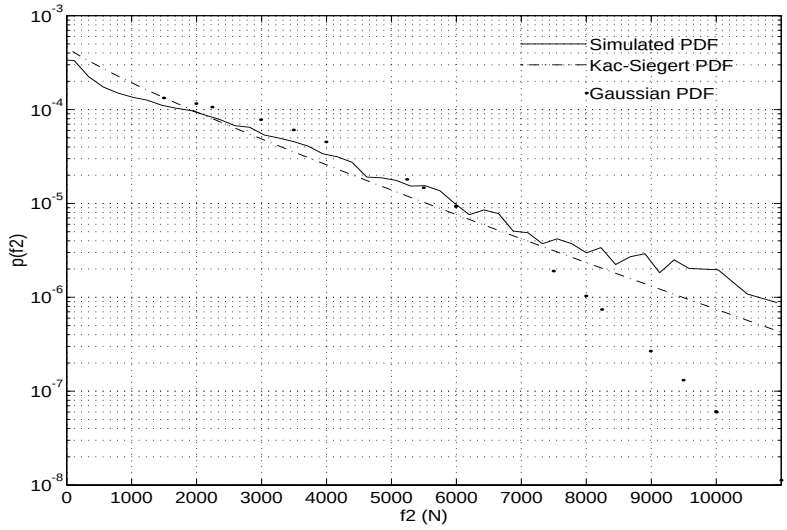

Figure 8: Comparison of Kac-Siegert and simulated pdfs for heave force

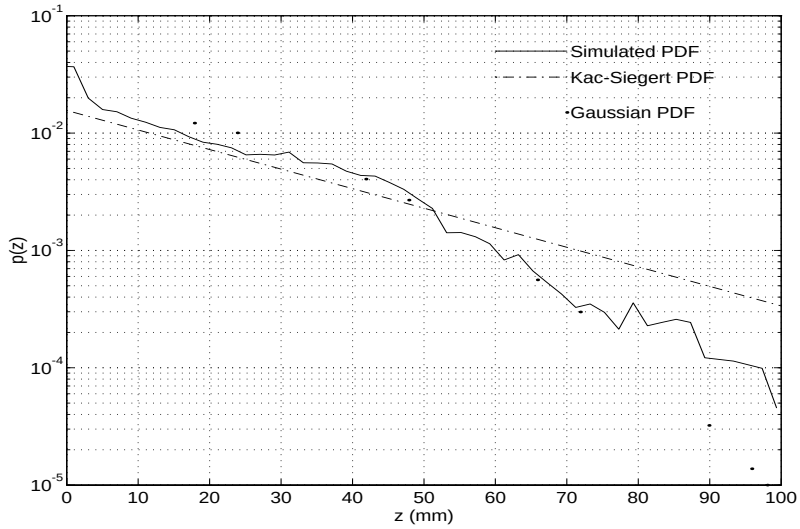

Figure 9: Comparison of Kac-Siegert and simulated pdfs, damping=0.05%

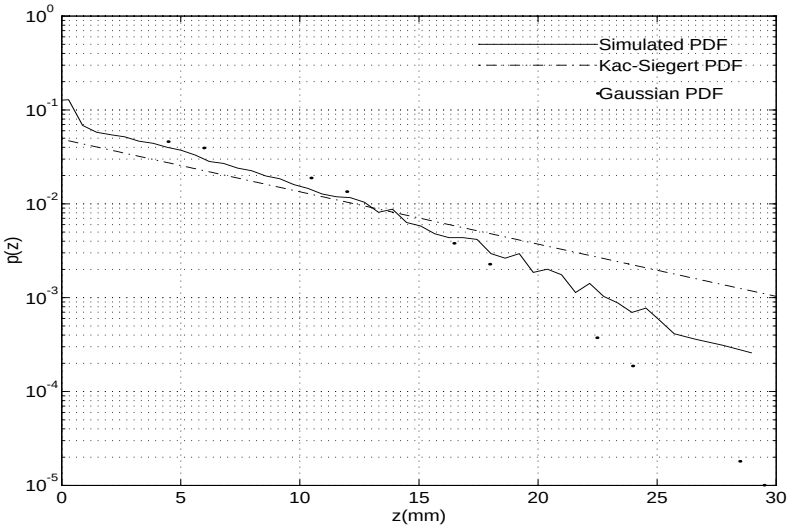

Figure 10: Comparison of Kac-Siegert and simulated pdfs, damping=0.15%

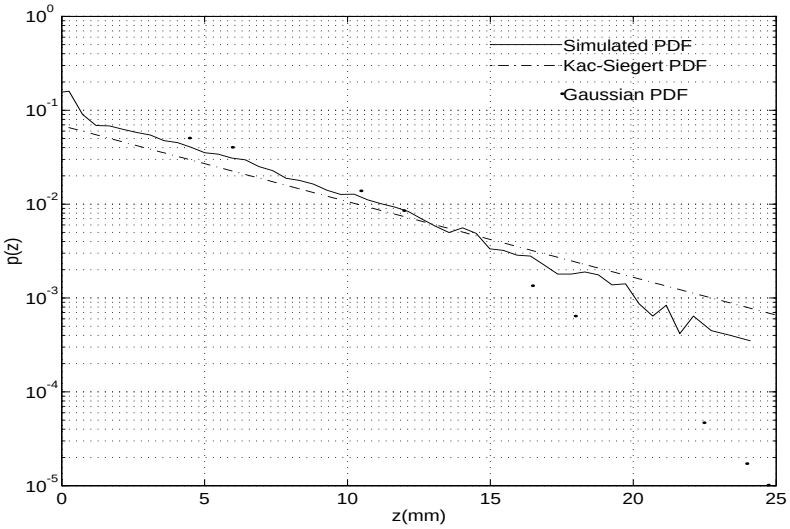

Figure 11: Comparison of Kac-Siegert and simulated pdfs, damping=0.20%

simulation can be compared with the PDFs obtained from the Kac-Siegert analysis. The numerically generated and analytically based PDFs are presented on semi-logarithmic axes and compared with a Gaussian distribution in Figure 8 for heave force, and in Figures 9 to 11 for heave response for three levels of damping (0.05, 0.15 and 0.20 %). The results for second order force show good agreement between the simulated and analytically generated PDFs. The heave response results show increasingly close agreement as the assumed damping is increased. A similar conclusion was reached by Stansberg (1991) in the case of low frequency drift responses: he found that his simplified model offered close agreement with simulated PDFs at high levels of damping, but performed less well for lightly damped responses.

In conclusion, this section has described a methodology for estimating the probability density function of second order forcing or response by representing the process as a weighted sum of sub-processes which themselves are the squares of mean zero, unit variance Gaussian processes. Comparisons have also been made with statistics estimated from direct simulations. Further work is required to clarify the reliability of the statistics thereby obtained.

Acknowledgements

This work received support from the Engineering and Physical Sciences Research Council, through grants GR/J23167 and GR/L19355 and a research studentship held by the second author. The analysis in section 2, and most of the computations therein, were undertaken by Dr J. B. Huang.

References

[1] E.C. Bowers. Long period oscillations of moored ships subject to short wave seas. *Transactions of the Royal Institution of Naval Architects*, 118:181–191, 1976.

[2] M. Brooking and E.R. Jefferys. Experience of single tether buoy dynamics. In *Proceedings of the First European Offshore Mechanics Symposium (EUROMS90), Trondheim, Norway*, pages 252–264, 20-22 August 1990.

[3] F.P. Chau. *The second order velocity potential for diffraction of waves by fixed offshore structures.* PhD thesis, Department of Mechanical Engineering, University College London, 1989.

[4] F.P. Chau and R. Eatock Taylor. Second-order velocity potential for arbitrary bodies in waves. In *Proceedings of the 3rd International Workshop on Water Waves and Floating Bodies, Woods Hole, Mass.*, pages 15–19, 1988.

[5] F.P. Chau and R. Eatock Taylor. Second order wave diffraction by a vertical cylinder. *Journal of Fluid Mechanics*, 240:571–599, 1992.

[6] X. B. Chen, B. Molin, and F. Petitjean. Faster evaluation of resonant excitation loads on tension leg platforms. In *Proceedings of the 8th International Symposium on Offshore Engineering, Brazil*, pages 427–441, 1991.

[7] X.B. Chen and B. Molin. Vertical resonant motions of tension leg platforms. Interim Report 24841, Institut Francais de Petrole, 1990.

[8] R. Eatock Taylor. Assessment of springing in tension leg platforms. In C.S. Smith and R.S. Dow, editors, *Advances in marine structures - 2*, pages 174–207. Elsevier Applied Science, 1991.

[9] R. Eatock Taylor and F.P. Chau. Wave diffraction theory - some developments in linear and nonlinear theory. *Journal of Offshore Mechanics and Arctic Engineering*, 114:185–194, 1992.

[10] R. Eatock Taylor and J.B. Huang. Second order wave diffraction by an axisymmetric body in monochromatic waves. *Proceedings of the Royal Society*, 453:1515–1541, 1997a.

[11] R. Eatock Taylor and J.B. Huang. Semi-analytical formulation for second order diffraction by a vertical cylinder in bichromatic waves. *Journal of Fluids and Structures*, 11:465–484, 1997b.

[12] R. Eatock Taylor and S.M. Hung. Second-order diffraction forces on a vertical cylinder in regular waves. *Applied Ocean Research*, 9(1):19–30, 1987.

[13] S.A. Ghalayini and A.N. Williams. Non-linear wave forces on vertical cylinder arrays. *Journal of Fluids and Structures*, 5:1–32, 1991.

[14] J.B. Huang and R. Eatock Taylor. Semi-analytical solution for second order wave diffraction by a truncated circular cylinder in monochromatic waves. *Journal of Fluid Mechanics*, 319:171–196, 1996.

[15] J.B. Huang and R. Eatock Taylor. Evaluation of second order forces on an array of truncated cylinders by a semi-analytical method. In *Proceedings of the Sixteenth International Symposium on Offshore Mechanics and Arctic Engineering*, 1997.

[16] M. Kac and A.J.F. Siegert. An explicit representation of a stationary gaussian process. *Annals of Mathematical Statistics*, 18:438–442, 1947a.

[17] M. Kac and A.J.F. Siegert. On the theory of noise in radio receivers with square law detectors. *Journal of Applied Physics*, 18:383–397, 1947b.

[18] S. Kato, T. Kinoshita, and S. Takase. Statistical theory of total second order responses of moored vessels in random seas. *Applied Ocean Research*, 12(1):2–13, 1990.

[19] M. P. Kernot. *The second order forcing and response of offshore structures in irregular seas.* PhD thesis, Department of Engineering Science, University of Oxford, 1995.

[20] M.H. Kim. Second-order, sum-frequency wave loads on large volume structures. *Applied Ocean Research*, 13(6):287–296, 1991.

[21] M.H. Kim and D.K.P. Yue. The complete second-order diffraction solution for an axisymmetric body. part 1. monochromatic incident waves. *Journal of Fluid Mechanics*, 200:235–264, 1989.

[22] M.H. Kim and D.K.P. Yue. The nonlinear sum-frequency wave excitation and response of a tension-leg platform. In *Proceedings of the International Conference on the Behaviour of Offshore Structures (BOSS '88)*, volume 2, pages 687–703, June 1988.

[23] D.L. Kriebel. Non linear wave interaction with a vertical circular cylinder, part ii: wave run-up. *Ocean Engineering*, 19:75–99, 1992.

[24] R.S. Langley. On the time domain simulation of second order wave forces and induced responses. *Applied Ocean Research*, 8(3):134–143, 1986.

[25] R.S. Langley. Second order frequency frequency domain analysis of moored vessels. *Applied Ocean Research*, 9(1):7–18, 1987.

[26] R.S. Langley and S. McWilliam. A statistical analysis of first and second order vessel motions induced by waves and wind gusts. *Applied Ocean Research*, 15(1):13–23, 1993.

[27] C.-H. Lee and J.N. Newman. Second-order wave effects on offshore structures. In *Proceedings of the 7th International Conference on the Behaviour of Offshore Structures (BOSS '94)*, volume 2, pages 133–145, 1994.

[28] C.-H. Lee, J.N. Newman, M.H. Kim, and D.K.P. Yue. The computation of second-order wave loads. *Journal of Offshore Mechanics and Arctic Engineering*, 114:113–123, 1991.

[29] J. Lighthill. Waves and hydrodynamic loading. In *Proceedings of the 2nd International Conference on the Behaviour of Offshore Structures (BOSS '79), London*, pages 1–39, 1979.

[30] Y-K.M. Lin. *Probabilistic Theory of Structural Dynamics*. McGraw-Hill, New York, 1967.

[31] C.M. Linton and D.V. Evans. The interaction of waves with arrays of vertical circular cylinders. *Journal of Fluid Mechanics*, 215:549–569, 1990.

[32] Y.H. Liu, C.-H. Kim, and X.S. Lu. Comparison of higher order boundary element and constant panel methods for hydrodynamic loading. In *Proceedings of the First European Offshore Mechanics Symposium (EUROMS90), Trondheim, Norway*, 20-22 August 1990.

[33] Š. Malenica. Second-order interaction of water waves with arrays of vertical cylinders. In *Proceedings of the 2nd Congress of Croatian Society of Mechanics, Supetar, Croatia*, pages 599–606, 1997.

[34] T. Marthinsen and J. Muren. Snorre TLP : comparison of measured and predicted response. In M.H. Patel, editor, *Proceedings of the Seminar on Tension Buoyant Platforms*. Bentham Press, 25-26 May, 1993.

[35] T. Matsui, T. Susuki, and Y. Sakoh. Second order diffraction forces on floating bodies in regular waves. In *Proceedings of the First Pacific/Asia Offshore Mechanics Symposium*, 1990.

[36] S. McWilliam and R.S. Langley. Extreme values of first- and second-order wave-induced vessel motions. *Applied Ocean Research*, 15(4):169–181, 1993.

[37] S. McWilliam and R.S. Langley. Response statistics of non-linearly moored vessels under the action of first and second order wave forces. *Applied Ocean Research*, 16(4):295–311, 1994.

[38] C.C. Mei. *The Applied Dynamics of Ocean Surface Waves*. World Scientific Publishing Co., 2nd edition, 1992.

[39] B. Molin. Second-order diffraction loads upon three-dimensional bodies. *Applied Ocean Research*, 1(4):197–202, 1979.

[40] W.I. Moubayed and A.N. Williams. Second order hydrodynamic interactions in an array of vertical cylinders in bichromatic waves. *Journal of Fluids and Structures*, 9:61–98, 1995.

[41] A. Naess. Statistical analysis of second-order response of marine structures. *Journal of Ship Research*, 29(4):270–284, 1985.

[42] A. Naess. The statistical distribution of second-order slowly-varying forces and motions. *Applied Ocean Research*, 8(2):110–118, 1986.

[43] A. Naess. Prediction of extremes of combined first-order and slow-drift motions of offshore structures. *Applied Ocean Research*, 11(2):100–110, 1989.

[44] A. Naess. Statistical analysis of nonlinear, second-order forces and motions of offshore structures in short crested random seas. *Probabilistic Engineering Mechanics*, 5(4):192–203, 1990.

[45] A. Naess and J.M. Johnsen. Response statistics of nonlinear, compliant offshore structures by the path integral solution method. *Probabilistic Engineering Mechanics*, 8(2):91–106, 1993.

[46] A. Naess and G.M. Ness. Second-order, sum-frequency response statistics of tethered platforms in random waves. *Applied Ocean Research*, 14(1):23–32, 1992.

[47] B. Natvig. Tensioned buoyant platforms : hydrodynamic design. In M.H. Patel, editor, *Proceedings of the Seminar on Tension Buoyant Platforms*. Bentham Press, 25-26 May, 1993.

[48] E. Neal. Second-order hydrodynamic forces due to stochastic excitation. In R.D. Cooper and S.W. Doroff, editors, *Proceedings of the Tenth Symposium on Naval Hydrodynamics: Hydrodynamics for Safety and Fundamental Hydrodynamics*, pages 517–539. Office of Naval Research and the U.S. Coast Guard, 24-28 June, 1974. Cambridge, Massachusetts, USA.

[49] D.E. Newland. *An introduction to Random vibrations, spectral and wavelet analysis*. Longman Scientific and Technical, 3nd edition, 1993.

[50] J.N. Newman. The second harmonic wave force on a vertical cylinder. *Journal of Fluid Mechanics*, 320:417–443, 1996.

[51] F. Noblesse. Integral identities of potential theory of radiation and diffraction of regular waves by a body. *Journal of Engineering Mathematics*, 17:1–13, 1983.

[52] T.F. Ogilvie. Second-order hydrodynamic effects on ocean platforms. In *Proceedings of the International Workshop on Ship and Platform Motions, Berkeley, Ca.*, pages 205–265, 1983.

[53] A. Papoulis. *Probability, Random Variables and Stochastic Processes.* McGraw-Hill Book Co., 3rd edition, 1991.

[54] C. Petrauskas and S.V. Liu. Springing force response of a tension column platform. In *Proceedings of the 19th Offshore Technology Conference*, 1987. OTC 5458.

[55] W.G. Price and R.E.D. Bishop. *Probabilistic theory of ship dynamics.* Chapman and Hall, 1974.

[56] J.B. Roberts. Nonlinear analysis of slow drift oscillations of moored vessels in random seas. *Journal of Ship Research*, 25(2):130–140, 1981.

[57] T. Sarpkaya and M. Isaacson. *Mechanics of wave forces on offshore structures.* Van Nostrand Reinhold, New York, 1981.

[58] M. Schetzen. *The Volterra and Wiener theories of nonlinear systems.* John Wiley and Sons, 1980.

[59] C.T. Stansberg. A simple method for estimation of extreme values of non-gaussian slow-drift responses. In *Proceedings of the First International Offshore and Polar Engineering Conference, Edinburgh, UK*, pages 442–451, 11-16 August 1991.

[60] B. Teng and S. Kato. An efficient method for second-order velocity potential: towards the calculation of third order forces. In *Proceedings of the 11th International Workshop on Water Waves and Floating Bodies, Hamburg*, 1995.

[61] M.J. Tucker, P.G. Challenor, and D.J.T. Carter. Numerical simulation of a random sea: a common error and its effect upon wave group statistics. *Applied Ocean Research*, 6(2):118–122, 1984.

[62] T. Vinje. On the statistical distribution of second-order forces and motions. *International Shipbuilding Progress*, 30:58–68, 1983.

[63] O.C. Zienkiewicz. *The Finite Element Method.* McGraw-Hill, 1977.